MODELLING WAVES AND CURRENTS IN NORTHEASTERN LAKE ONTARIO TO ASSESS THE IMPACTS OF A PROPOSED OFFSHORE WIND FARM

by

Matthew McCombs

A thesis submitted to the Department of Civil Engineering

In conformity with the requirements for

the degree of Masters of Applied Science

Queen's University

Kingston, Ontario, Canada

(September, 2013)

Abstract

A spectral wave model (SWAN) coupled with a depth averaged hydrodynamic model (Delft3D) was used to understand the wave and flow dynamics of the Kingston Basin of Lake Ontario during large winter storm events. This model was then used to assess the impact of an offshore wind farm in the Kingston Basin. Results over different model domains with various forcing methods were compared to achieve the highest correlation with wave, current and water level observations from several locations. Storm events were modelled over the complex bathymetry of the basin and results were verified using wave and current profiler data collected during the winters of 2009-10 and 2011-12. Waves were composed of both locally generated wind sea and swell from the main basin of Lake Ontario, while flows throughout the Kingston Basin showed a complex circulation pattern. This circulation is composed of several wind-driven gyres, which are magnified during storm events. The impact of waves on the circulation patterns within the basin is highest in shallow areas where wave breaking drives circulation. To simulate a wind farm, a transmission coefficient was used in the wave model to represent the effects on waves, and an energy loss term was added to the hydrodynamic momentum equations to represent the added drag of the piles on the circulation. The results indicate that the coastal areas in eastern Lake Ontario will be minimally affected. The headlands of Big Sandy Bay, Wolfe Island, could see the largest coastal effects with changes in significant wave height predicted to be < 2%. The majority of impacts to circulation occur in the near-field, with changes in current magnitude of < 0.08 m s^{-1} (up to 50%). Areas near Wolfe Island exhibit changes of ~ 0.05 m s^{-1} (30 %), although overall circulation patterns throughout the basin are not affected. The majority of changes to surface waves and wind-driven currents are due to wind farm position with respect to wind direction and the re-direction of flows and waves as they pass through the wind farm.

Co-Authorship

Significant contributions have been made by Leon Boegman and Ryan Mulligan by direct supervision of work, interpreting the results and commenting on the original work of Matthew McCombs for journal preparation. Yerubandi R. Rao has provided observations of various instruments and helped to better interpret the results for journal preparation.

Chapter 2 of this thesis has been published as:

McCombs, M.P., Mulligan, R.P., Boegman, L., Rao, Y.R. (2013). Wave Propagation and Growth in the Kingston Basin of Eastern Lake Ontario. *CSCE 4th Special Conference on Coastal, Estuary and Offshore Engineering.* COS-009, 1-8.

Chapter 3 of this thesis has been submitted as:

McCombs, M.P., Mulligan, R.P., Boegman, L., Rao, Y.R. (2013). Modelling Winter Storm Surface Waves and Wind-Driven Circulation in Eastern Lake Ontario. *J. Great Lakes Res.* Submitted.

Chapter 4 of this thesis has yet to be submitted.

Preface

This thesis has been organised as a series of manuscripts. As a result there is some overlap in the material presented in each chapter. The following text briefly clarifies the differences between chapters.

Chapter 2 involves the use of the wave model SWAN to simulate waves. A model domain of the Kingston Basin was used with an open boundary in the Rochester Basin of Lake Ontario. Two storms (named AS2 and BS3) were the focus of this chapter.

In Chapter 3, SWAN was coupled with the hydrodynamic model Delft3D to simulate waves, currents and water levels. In this chapter the model domain of the Kingston Basin, with an open boundary condition used in Chapter 2, was used and compared to a lake-wide model domain. Five storms were analysed (AS1-2 and BS1-3) and two of the storms (AS1 and BS1) were investigated in detail, different events than those investigated in Chapter 2.

Finally, Chapter 4 utilises the lake-wide domain in Chapter 3 and local wind forcing of storm BS3 to model the impacts of an offshore wind farm in the Kingston Basin.

Acknowledgements

I would like to thank my supervisors Leon Boegman and Ryan Mulligan for their support and guidance over the past two years. Their flexibility and availability were invaluable in the completion of this thesis. My colleagues in the hydrotechnical group were always available for help and support with everything from suggestions during seminar presentations, to help with plotting figures. Reza, Damien, Shastri, Payam, Neville, Nadira, Aidin, Nader, Logan, Greg, Hadiseh and Myles all deserve recognition for their help in the completion of this thesis.

Special thanks to my wife Courtney for her love and patience with me over the last six years, and to my parents Patrick and Diane for their never-ending support and encouragement. I would also like to thank my undergraduate friends here at Queen's Sean, Chris and Mike who decided to stick around for an extra couple of years just to be with me.

I would also like to thank Baird and Associates Ltd. for the use of their AWAC observations, especially to Andrew McGillis for his helpful suggestions and encouragement. I would also like to thank the crew at Environment Canada, especially Ram Yerubandi for the deployment and retrieval of several instruments used for this thesis. This research was funded by the Ontario Ministry of Research and Innovation Early Researcher Award to LB, by Environment Canada and an NSERC Discovery Grant to RM.

Table of Contents

List of Figures

List of Tables

Chapter 1

Introduction

1.1 Background

The Great Lakes of North America contain a significant portion of the world's freshwater. The lakes are an invaluable resource to Canada and the United States and a host to delicate ecosystems which need to be studied and protected. At present, urban development around the Great Lakes continues and in the future the need for renewable energy may result in the construction of offshore wind farms. An understanding of the current state of the Great Lakes is, therefore, needed to assess the impacts of implementing wind farms in the future. Detailed numerical modelling techniques combined with wave and current observations in the lakes and reviewing past studies are commonly used methods for evaluating such impacts.

Circulation in the Great Lakes has been described and modelled in past studies. The focus of this thesis is to understand the waves and circulation of Lake Ontario (Figure 1.1). From observations and numerical models of the Great Lakes (e.g. Picket, 1980; Simon and Murthy, 1985; Beletsky et al., 1999), it is known that a double gyre circulation forms in Lake Ontario. This pattern is composed of clockwise flow in the north and counter clockwise flow in the south. This circulation pattern is stronger during the winter seasons and is almost entirely wind driven (Beletsky et al. 1999).

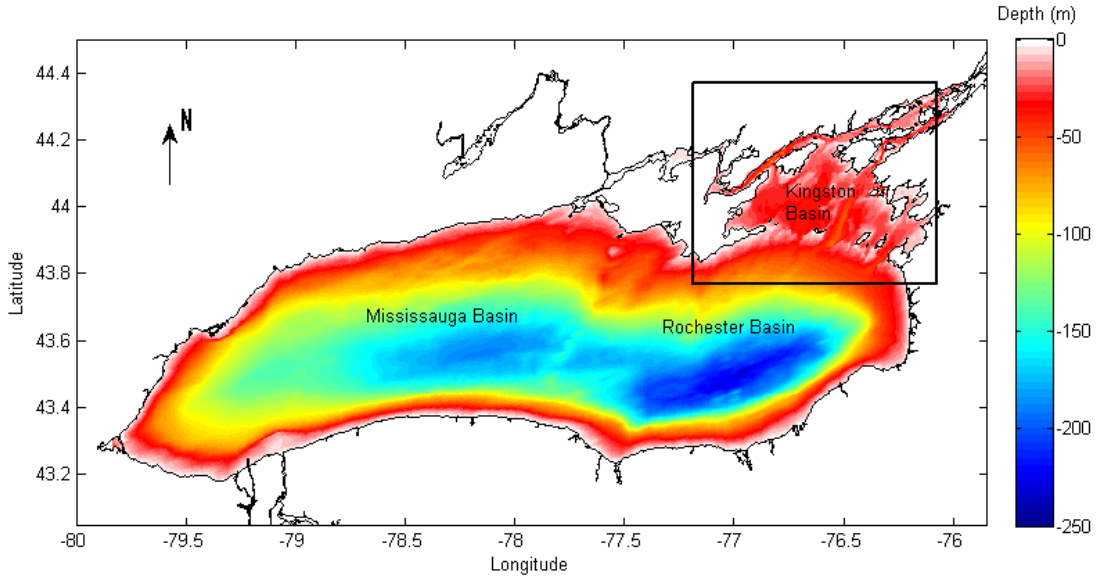

Figure 1.1: Bathymetry of three basins of Lake Ontario (NOAA, 2013) with the Kingston Basin outlined by the black box.

Coupled surface waves and currents are modelled coarsely (5 km resolution) over the Great Lakes by the Great Lakes Coastal Forecasting System (GLCFS), which is based on the finite difference Princeton Ocean Model (POM) and the Donelan wave model (see Schwab et al., 1984 and Bedford and Schwab, 1991). This modelling system provides, for other researchers, modelled hourly wave and current data for the Great Lakes. Modelling attempts focusing solely on Lake Ontario have also been performed in the past (e.g. Prakash et al., 2007; Huang et al., 2010).

Flow distribution and circulation through the Kingston Basin have been described by Tsanis and Murthy (1990), and by Tsanis et al. (1991), who observed the mean currents in the Kingston Basin over the summer months. The basin has been modelled by Paturi et al. (2012; using ELCOM (Estuary and Lake Computer Model), to examine the stratified flows during the summer and fall months, and by Shore (2009); using FVCOM (Finite Volume Coastal Ocean

Model), to investigate the circulation and exchange between the Kingston Basin and Lake Ontario. These two studies found that winds commonly induce gyres in the Kingston Basin, and the predominant circulation patterns can reverse under certain wind conditions.

State-of-the-art wave models solve the spectral action balance equation using source terms that account for wave generation by wind, non-linear (three-wave and four-wave) interactions, which evolve the shape of the wave spectrum (see Booij et al., 1999), and wave energy dissipation (wave breaking, whitecapping, and bottom friction). The wave model Simulating Waves Nearshore (SWAN; Booij et al., 1999) is used throughout this thesis to simulate the wave field through the Kingston Basin. SWAN has been used in other studies to simulate waves over steep and complex bathymetry (e.g. Gorrell et al., 2010). Delft3D (Lesser et al., 2004) is a 3-Dimensional (3D) hydrodynamic model that can simulate wave-current interactions by coupling the flow module with SWAN. This modelling suite has been used in several studies successfully (e.g. Mulligan et al., 2010; Elias et al., 2012) and in this thesis. Once waves and currents are understood and storms can be simulated through a validated model, offshore wind farms can be added to the model for comparison.

The Ontario government imposed a moratorium, in August of 2011, declaring that offshore wind farm impacts in Lake Ontario require further scientific research (CBC News, 2011). Although many offshore wind projects have been carried out in coastal areas in Europe (e.g. Scroby Sands; CEFAS, 2006, Horn Rev and Nysted; Danish Energy Autority, 2006), wind farm impacts on freshwater systems are less well understood. Lake Vanern in Sweden contains a wind farm, although the scale of the lake (5,655 km^2) and the farm (10 turbines), compared to what has previously been proposed for Lake Ontario (18,960 km^2), is small (130 turbines). Scientific and technical issues associated with potential offshore wind farm development in North

America have been studied (Baird, 2011; Manwell et al., 2007), highlighting the issues involving wind farms in the Great Lakes. This work is a first step toward modelling the impacts of offshore wind farms in the Great Lakes.

1.2 Importance of Research

Most of the past modelling efforts in Lake Ontario have focused on summer circulation (e.g. Tsanis et al., 1991; Paturi et al., 2011). There is a need to investigate winter circulation and the wave climate within the lake, in order to understand the strongest annual events and, therefore the full seasonal cycle. In addition, the interaction of the wave and flow fields within the basin has not yet been studied.

The need to study wind farm development is clear as it is an alternative form of energy that may become essential in the future. Understanding the wave and current processes in Lake Ontario will allow, for example, numerical modelling of the impact of offshore wind farms on the waves and circulation in Lake Ontario. Modelling large storm events will help identify the maximum impacts of farm development on the lake. This thesis describes a modelling system developed to investigate waves and currents during winter storms and how coastal processes are impacted by the construction of an offshore wind farm.

1.3 Thesis Objectives and Outline

The main objectives of this thesis are to: (1) construct and validate a surface wave model of the Kingston Basin of Lake Ontario, using measurements made during winter storm events, and use the results to further understand waves and in the Kingston Basin, (2) to use various forcing techniques to couple the wave model with a hydrodynamic model to investigate the relationship between waves and currents and understand winter circulation in the Kingston Basin, and (3) use the validated model to assess the changes in the wave field and circulation due to an

offshore wind farm. These topics are covered in the following three chapters of this thesis. Chapter 2 covers the use of the SWAN wave model to simulate waves in the Kingston Basin. Chapter 3 compares the model used in Chapter 2 to a lake-wide modelling approach and further defines the wave field and circulation of the Kingston Basin using both SWAN and the Delft3D hydrodynamic model. Chapter 4 introduces a modelling technique for representing an offshore wind farm in Lake Ontario and assessing the impact of such a farm on wave and currents in the coupled model. Conclusions and recommendations for future works are provided in Chapter 5.

Chapter 2

Wave Propagation and Growth in the Kingston Basin of Eastern Lake Ontario

2.1 Introduction

State-of-the-art wave models solve the spectral action balance equation using source terms such as wind stress, three-wave interactions, four-wave interactions, and dissipation (wave breaking, whitecapping, and bottom friction). The wave model SWAN (Booij et al., 1999) is used in this chapter to simulate the wave field through the Kingston Basin (the northeastern portion of Lake Ontario and headwaters of the St. Lawrence River). SWAN has been used in other studies to simulate waves over steep and complex bathymetry. As an example, Gorrell et al. (2010) found that SWAN accurately predicted the propagation of observed gravity waves to the shoreline over complicated near-shore bathymetry that included a steep submarine canyon in California. The Kingston Basin (Figure 2.1) is also composed of complicated topography including many islands and shoals protecting it from large waves in the main basin of the lake (see Sly and Prior, 1984). Two deep channels exist around these islands which affect wave propagation. The channel on the east side of Main Duck Island (see Figure 2.1) is named the Saint Lawrence Channel and on the west is the Simcoe Island Channel. The Saint Lawrence Channel reaches 56.2 m in depth and the Simcoe Island Channel reaches 41.2 m in depth. The shoals and islands which protect the Kingston Basin form Duck-Galloo Ridge, which averages at a depth of approximately 15 m.

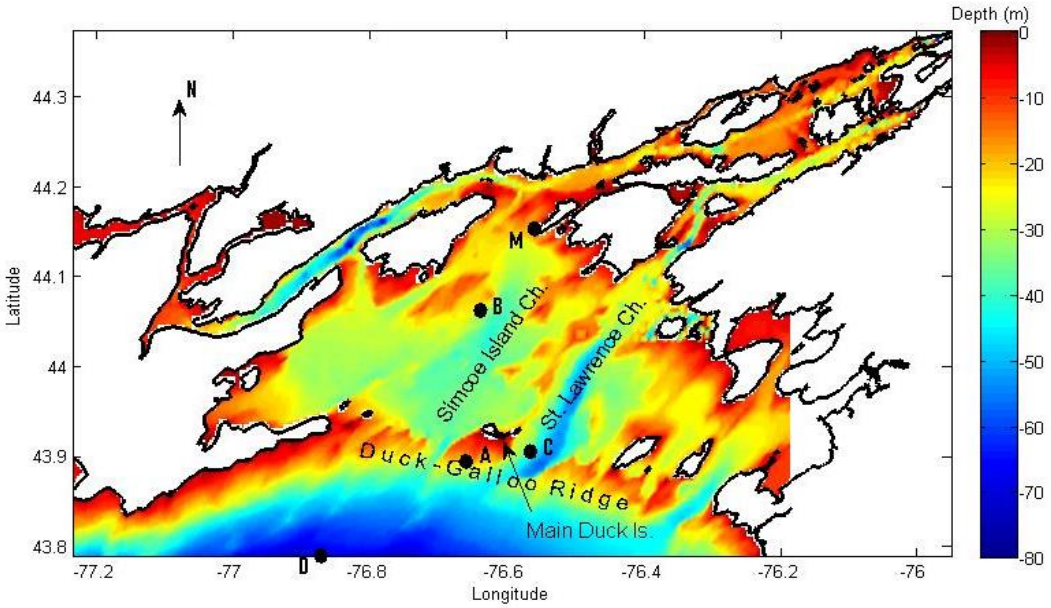

Figure 2.1: Bathymetry of eastern Lake Ontario (Kingston Basin and St. Lawrence River) based on Lake Ontario Datum (NOAA) and measurement locations: A. AWAC (1.2MHz) for the 2009-10 winter period at a depth of 18m. B. ADCP (600kHz) and TGR for the 2011-12 winter period at 26 m. C. TWR (4Hz) for the 2011-12 winter period at 42 m. D. Wave input location from NOAA Great Lakes Coastal Forecasting System at 68 m depth. M. Meteorological Station on Simcoe Island.

Flow distribution and circulation through the Kingston Basin have been described by Tsanis et al. (1990, 1991) and modelled by Paturi et al. (2012). Shore (2009) modeled the flow through Lake Ontario and identified the seasonal flow regimes affecting the Kingston Basin. Bottom sediments in the Kingston Basin have been studied by Gilbert (1999) who defined three sediment environments and found that the sediment distribution throughout the basin was primarily affected by wave energy. Although seasonal flows have been well documented, the wave field during storm events is not well understood.

The purpose of this chapter is to validate the SWAN model and use the predictions to understand the wave field through the Kingston Basin. This will be the first step towards

numerically modelling the impact of a proposed offshore wind farm on waves and currents through the Kingston Basin. The wave field is described by comparing water depth and wave energy density from the main basin of Lake Ontario and eastward through the Kingston Basin towards the head of the St. Lawrence River.

2.2 Observations

The model was forced with wave data from the Great Lakes Coastal Forecasting System (GLCFS; Schwab, 1994) at site D (location of the NDBC Prince Edward Point Buoy) along the southern boundary and compared with field observations within the Kingston Basin and along the Duck-Galloo Ridge (Figure 2.1). The waves simulated by the GLCFS at site D, the location of the Environment Canada Prince Edward Pt. buoy (not deployed in the winter months), were presumed to be a good representation of wave conditions across the southern boundary. Observational data was collected over two winter periods. The 2009-10 winter observations were made using a Nortek AWAC (acoustic wave and current profiler, Figure 2.1, site A); data was provided by W.F. Baird & Associates Coastal Engineering Ltd., which captured two storm events (Figure 2.2, AS1 and AS2). These two events were simulated to ensure accurate representation by the model of the waves at Duck-Galloo Ridge outside the basin. The 2011-12 winter observations were made with an RDI ADCP (acoustic Doppler current profiler) at site B, and RBR TGR and TWR (pressure sensors) deployed by Environment Canada (at sites B and C, respectively). During this period a meteorological station was located at Nine Mile Point on Simcoe Island (site M) and the wind observations were used to force the model for the 2011-12 winter storms (Figure 2.2, BS1, BS2 and BS3). These events were validated to ensure accurate representation by the model of the waves inside the Kingston Basin (site B).

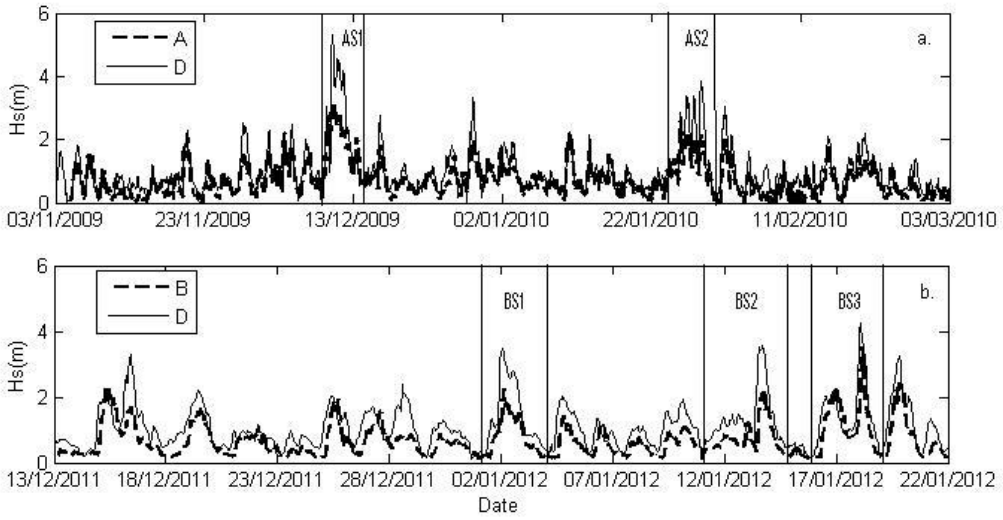

Figure 2.2: Time series of significant wave height (H_s) for each winter period (a. 2009-10 and b. 2011-12) at various locations (sites A, B, and D). The two storms of interest for this chapter are AS2 and BS3. Results for the other storms will be presented elsewhere (chapter 3).

Wind and wave forcing came from the GLCFS including significant wave heights, H_s, wave period, T_p, and wave direction, θ_p. The GLCFS time series (D) as well as AWAC (A) and ADCP (B) observations of significant wave height for the two winter periods observed are shown in Figure 2.2. In this chapter, storms AS2 and BS3 are compared and used to understand the wave conditions inside and outside the Kingston Basin. The wind and wave inputs for the two storms are provided in Figure 2.3. Strong northwesterly winds of up to 20 m s^{-1} for storm BS3 produced waves with a significant wave height of up to 4m at the boundary (input from GLCFS at site D) of the model domain. The evolution of peak storm waves through the Duck-Galloo Ridge and into the Kingston Basin is shown and defined in section 2.4.

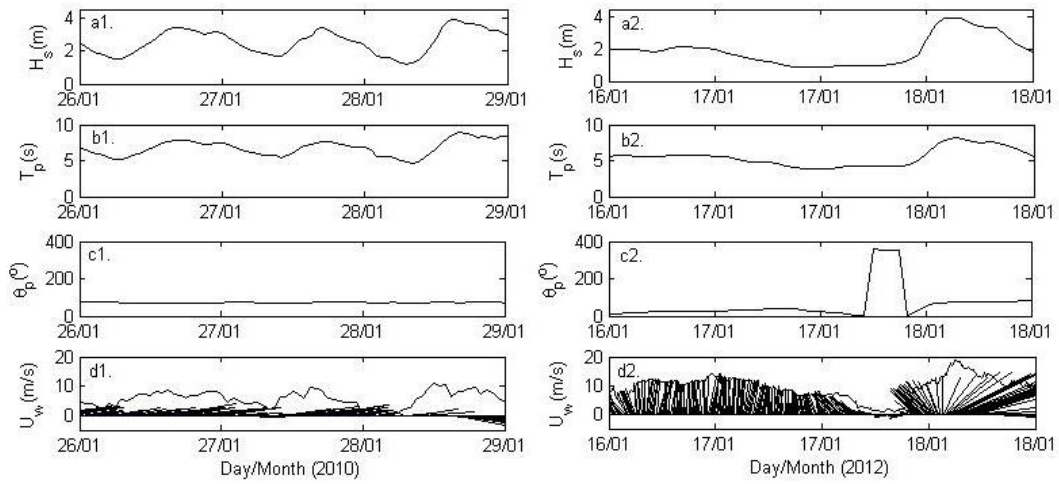

Figure 2.3: Storm AS2(1) and BS3(2) significant wave height (H_s, a), wave period (T_p, b), wave direction (θ_p, c) and wind speed and wind direction vectors (U_w, d).

2.3 Model Simulations

The spectral surface wave model SWAN is used to gain an understanding of the surface wave conditions within the Kingston Basin. The SWAN model computes the evolution of random waves and accounts for refraction, as well as wave generation due to wind, dissipation resulting from white capping, bottom friction and depth-induced wave breaking and non-linear wave-wave interactions (see Booij et al. 1999). The evolution of the wave field is described by the action balance equation (Equation 2.1). This computation provides its user with the propagation of wave action density in each dimension on the left-hand side and is balanced by local changes to the wave spectrum on the right-hand side:

$$\frac{\partial}{\partial t}N+\frac{\partial}{\partial x}c_x N+\frac{\partial}{\partial y}c_y N+\frac{\partial}{\partial \sigma}c_\sigma N+\frac{\partial}{\partial \theta}c_\theta N=\frac{S_{tot}}{\sigma} \qquad [2.1]$$

where t is time (s), c_x and c_y are spatial velocities in the x and y components (m s^{-1}), c_θ and c_σ are rates of change of group velocity which describe the directional (θ) rate of turning and frequency (σ) shifting due to changes in currents and water depth, N is wave action density spectrum, and

S_{tot} are the energy density source terms which describe local changes to the wave spectrum. The energy density source terms include wind, dissipation (whitecapping, bottom friction and depth-induced breaking) and nonlinear interactions (triads and quadruplets). SWAN was run with wave input along a boundary across the portion of the lake shown in Figure 2.1 at latitude 43.8°N. Wind from the MET station (Figure 2.1, site M) was forced uniformly through the spherical grid which contained grid cells with dimensions of 260 m (longitude) and 370 m (latitude).

The wave model was validated with error analysis of significant wave height, and wave period as well as wave spectral comparison of measurements and observations. A comparison of simulated to observed wave parameters is provided in Figure 2.4. Storm AS2 resulted in a RMSE (root mean squared error) for significant wave height of 0.32 m and an R value (correlation coefficient) of 0.80. For wave period, a RMSE of 1.20 s and an R value of 0.71 were observed. Storm BS3 resulted in a significant wave height RMSE of 0.26 m and R value of 0.95 and a wave period RMSE of 0.93 s and R value of 0.59.

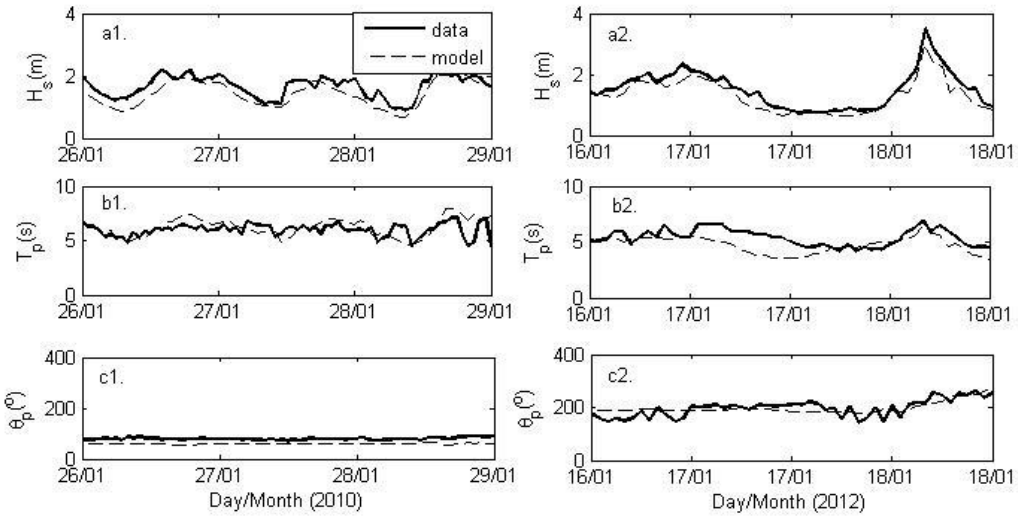

Figure 2.4: Simulation comparison with observations from the AWAC (site A) for storm AS2 (1) and from ADCP (site B) for storm BS3 (2) of various wave parameters: a. Significant Wave Height (H_s), b. Wave Period (T_p) and c. Wave Direction (θ_p).

The spectral wave comparison of observed waves (Obs) and simulated waves (Mod) is presented for different times at site A (outside the basin) and site B (inside the basin), in Figure 2.5. The wave spectrum is generally well replicated by the model. Storm BS3 provided better results as the wind data collected and forced into the model was more local and reliable (MET station on Simcoe Island). The number of peaks within the wave spectra is accurately represented by the model after comparison with the observations. At the time of maximum H_s for storm BS3 (Figure 2.5, b2) one spectral peak occurs in both simulated results and observations and two peaks are found in all other times shown. The frequencies at which these peaks occur is not as well represented in storm AS2 although this can be associated with discrepancies in estimated wind input (by GLCFS) to the model for the 2009-10 winter period when compared to measurements by the MET station within the Kingston Basin during the 2011-12 winter period, although both are acceptable inputs to the model which resulted in reasonable errors.

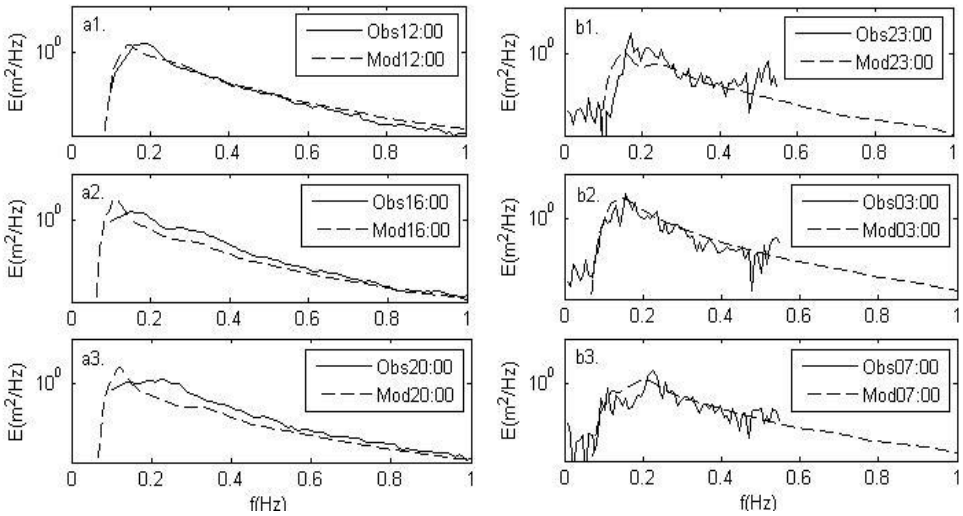

Figure 2.5: Comparison of surface elevation spectra for observations from the ADCP and AWAC (Obs a and Obs b, respectively) and SWAN simulations of storms AS2 (a) and BS3 (b) at storm peaks (2), four hours prior to storm peaks (1) and four hours after storm peaks (3). Peak for AS2 occurs on 28/01/2010 and for BS3, 18/01/2012.

2.4 Kingston Basin Wave Field

The simulated wave field at the peak of storm BS3 is shown in Figure 2.6. Significant wave height and wave direction vectors throughout the model domain are used to visualize wave progression. In conjunction with Figure 2.6, to help understand wave progression, is the plot of energy density as waves propagate into the Kingston Basin (Figure 2.7) and the spectral representations of waves in section 2.3 (Figure 2.5).

The spectral representations (Figure 2.5) suggest that two peaks are generally found in the wave spectrum at sites A and B. The first peak found between at < 0.2Hz and corresponds to swell waves, implemented at the boundary, moving into and throughout the Kingston Basin from the main basin of the lake. The second peak, > 0.2Hz, represents a transient wind-sea peak from wave growth due to winds over the Kingston Basin. During peak storm conditions (Figure 2.5, b2), one peak is found within the wave spectrum as winds head in a north-easterly direction

perpendicularly to the Duck-Galloo Ridge. The waves at this time are shown in Figure 2.6 with direction vectors which indicate that the waves at this time travel perpendicularly across the ridge and into the basin resulting in minimal reflection, explaining the single peak in the wave spectra at location B inside the basin in the Simcoe Island Channel. Observations indicate that when winds approach from different directions, waves propagate from the main basin (swell, eg. Figure 2.5, b2) and new waves are formed within the Kingston Basin (wind-sea, eg. Figure 2.5, b3). The combination of these two wave types is the cause for the two peaks found in the majority of the spectrum in Figure 2.5.

The wave field in Figure 2.6 represents the peak of storm BS3 and shows the distribution of waves into and throughout the basin. The Duck-Galloo Ridge causes waves to concentrate into the two channels on either side of Main Duck Island. Wave energy is lost crossing the ridge as waves break, shoal, diffract and refract over the islands spanning the ridge. The wave propagation inside the basin is complicated and varies widely throughout. As can be seen in Figure 2.6, waves rapidly dissipate as they pass over the ridge and refract throughout the model domain particularly in the center of the basin where a windfarm has been proposed.

The portion of wave energy (E) which passes over the Duck-Galloo Ridge and into the two channels on each side of Main Duck Island was determined using the following equation (e.g. Kamphuis, 2010):

$$E = \frac{1}{8}\rho g H_s^2 \qquad [2.2]$$

where ρ is the density of water (kg m^{-3}), g is acceleration due to gravity (m s^{-2}) and H_s is significant wave height (m). The energy density at the four cross-sections (Figure 2.6, a, b, c and d) is provided in Figure 2.7 with corresponding water depths.

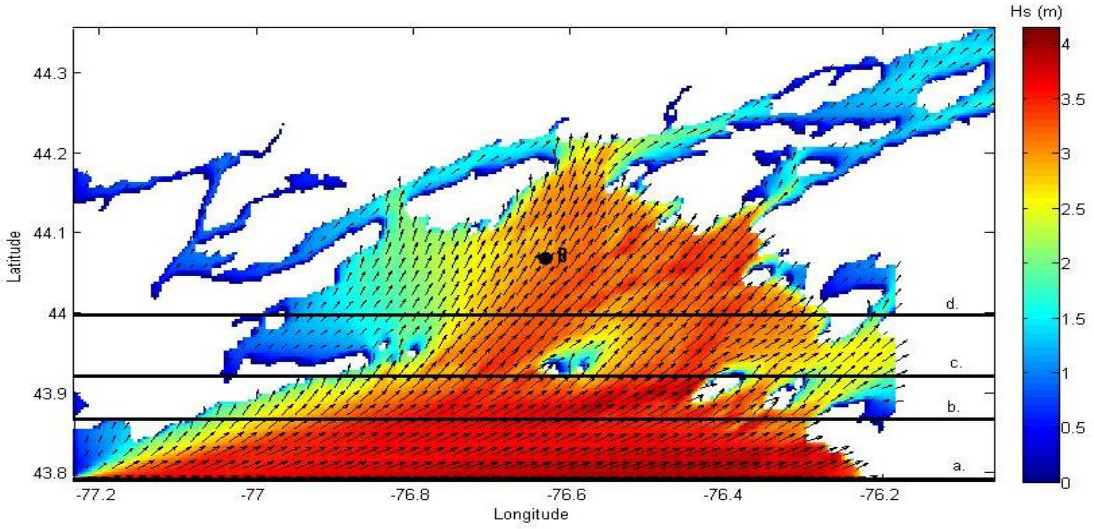

Figure 2.6: Significant wave height (H_s) and wave direction vectors, whose lengths indicate H_s magnitude, at the peak of storm BS3 (18/01/2012, 03:00). The locations of the four cross-sections referred to in Figure 2.7 are included (a, b, c and d).

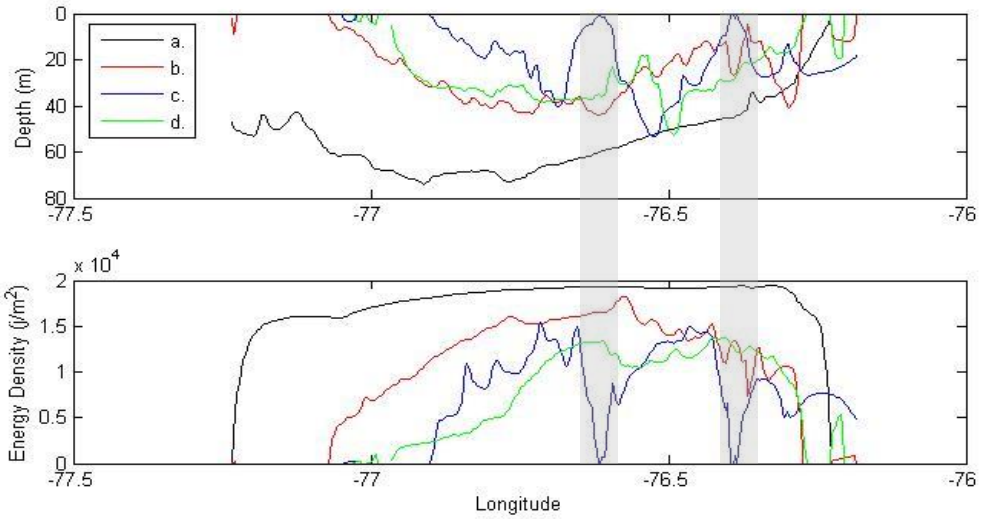

Figure 2.7: Water depth and wave energy density through cross-sections of the Kingston Basin. The locations of these are shown in Figure 2.6: a. southern boundary of model domain b. Just outside of Duck-Galloo Ridge in the main basin of Lake Ontario c. Through Duck-Galloo Ridge where the shaded areas represent the locations, along the longitudinal axis, of Main Duck Is. and Galloo Is. d. Inside the Kingston Basin at the peak of storm BS3 (18/01/2012, 03:00).

As waves propagate from south to north through the Kingston Basin, a reduction in energy density occurs towards the Duck-Galloo Ridge (Figures 2.6 and 2.7, b). Once waves reach the ridge, the energy density is reduced even further as energy is lost in the form of shoaling, breaking, and refracting (Figures 2.6 and 2.7, c). In this plot, two of the islands (Main Duck Island and Galloo Island) can be identified where the energy density reduces to zero. The influence of the two islands on the energy density of waves within the basin is less apparent as waves propagate into the Kingston Basin (Figures 2.6 and 2.7, d) and shorter period waves are generated by local wind. The largest waves entering the basin lose approximately 17% of their original wave energy density at the boundary due to the influence of the Duck-Galloo Ridge. Energy density continues to diminish as wave energy is lost with the progression of waves through the model domain toward the head of the St. Lawrence River.

2.5 Summary and Conclusions

A spectral wave model was used to simulate two storm wave events through the Kingston Basin in Eastern Lake Ontario, using wave input from greater Lake Ontario on the model boundary and wind-generation of waves over the model grid. This model was validated with observations at two locations collected over two winter periods.

At the peaks of the two storms, we determined that wave propagation from the main basin loses approximately 17% of their energy density due to breaking and refraction over Duck-Galloo Ridge. The percent loss of energy density was calculated by averaging the change in energy density south of the ridge in the main basin (cross-section b, Figure 2.7) to north of the ridge in the Kingston Basin (cross-section d, Figure 2.7) and dividing the change by the average energy density south of the ridge in the main basin. Within the basin, waves are composed of both swell and wind-sea resulting in significant wave heights up to approximately 3.5 m and peak

wave periods up to 7 s. During the largest storms identified, waves are driven by winds perpendicular to the Ridge, causing large waves composed predominantly of swell that enter the basin through Simcoe Island and St. Lawrence channels on both sides of Main Duck Island.

Understanding the wave field in the Kingston Basin will help to determine if the changes in waves due to offshore wind farm construction within the Kingston Basin impact the surrounding area, and may be applicable to future offshore wind farm consideration within the Great Lakes (see chapter 4). The flow field (chapter 3), sediment transport and coupling between surface dynamics and temperature stratification will be investigated in future studies.

Chapter 3

Modeling Surface Waves and Wind-Driven Circulation in Eastern Lake Ontario during Winter Storms

3.1 Introduction

Lake Ontario (Figure 3.1a) is comprised of three basins. The Mississauga Basin is located to the west, the Rochester Basin to the east, and the Kingston Basin at the northeastern end of the lake. The Kingston Basin (Figure 3.1b) contains complicated bathymetry including many islands and shoals protecting it from large waves produced in the main basin (Mississauga and Rochester Basins) of Lake Ontario. Two deep channels exist around these islands which affect wave and current propagation. The channel on the east side of Main Duck Island (Figure 3.1b) is named the St. Lawrence Channel (56.2 m deep) and on the west side is the Simcoe Island Channel (41.2 m deep). The shoals and islands, which protect the Kingston Basin form Duck-Galloo Ridge, have an average depth of approximately 15 m.

Circulation in the Great Lakes has been described and modelled in past studies. Pickett (1980) found that observed mean winter circulation patterns agreed with a steady-state, homogeneous model, driven with a wind from a direction of maximum response (from the west), and determined that circulation in Lake Ontario is, on average, composed of clockwise flow in the north and counter clockwise flow in the south. Simons and Murthy (1985) found similar patterns using a high resolution array of current meters in a north-south and east-west cross section in the Mississauga Basin of the lake. Beletsky et al. (1999) used long term (30 year) current observations to update climatological circulation maps and also found a two-gyre circulation pattern in Lake Ontario during the winter season. Winter circulation was found to be

almost entirely wind-driven and stronger than in the summer. Boyce et al. (1989) found that storm surges rarely exceed 0.5 m in Lake Ontario and observed similar circulation patterns to other studies. Hamblin (1982) observed four modes of surface seiching, including the fundamental mode of 5.06 hours.

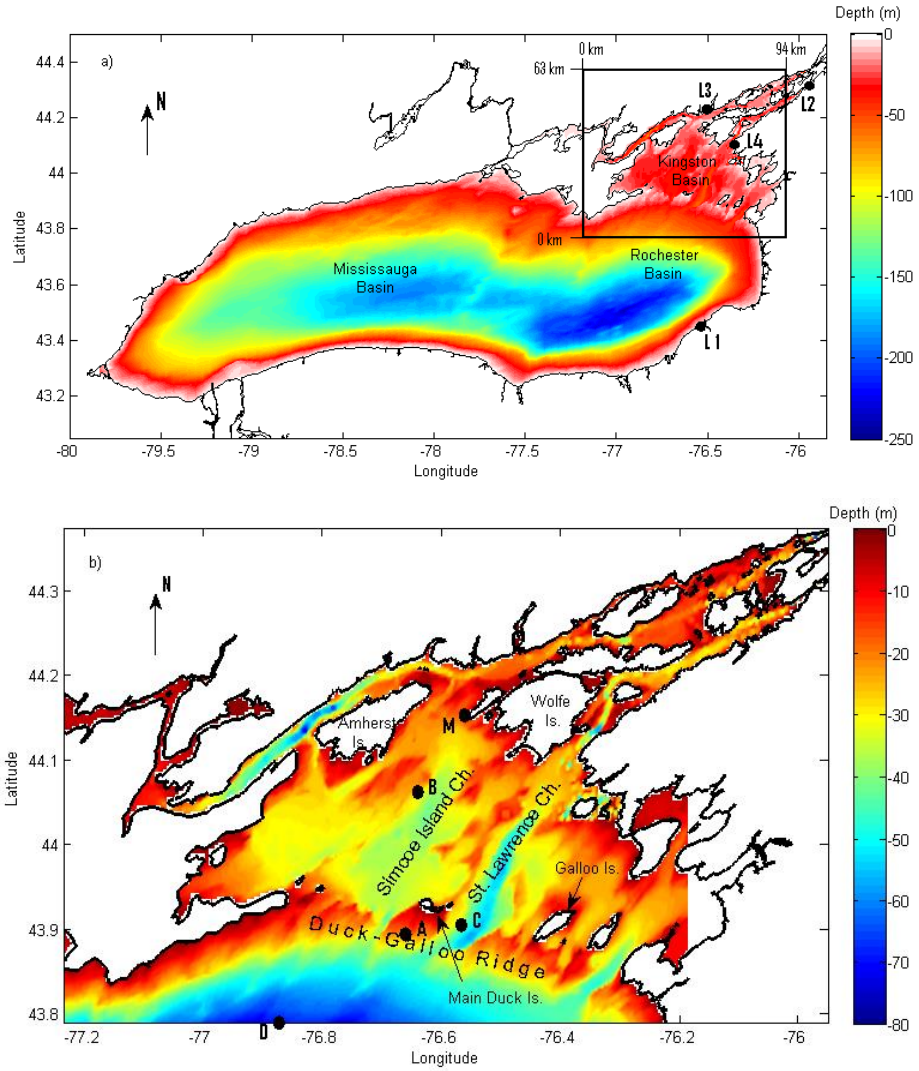

Figure 3.1: a) Bathymetry of Lake Ontario with the Kingston Basin outlined with dimensions. Water level input and comparison locations (L1-L4) are also provided with details in Table 3.2. b) Bathymetry of modelled eastern Lake Ontario (Kingston Basin and St. Lawrence River) based on NOAA (2013) and bathymetry used in Paturi et al. (2012). Observation sites are shown and details are provided in Table 3.1.

Numerical models of Lake Ontario have been used to investigate circulation in the past (e.g. Simons, 1974; Huang et al., 2010). Wave and currents are modelled coarsely (5 km resolution) over the Great Lakes by the Great Lakes Coastal Forecasting System (GLCFS), which is based on the finite difference Princeton Ocean Model (POM) and the Donelan wave model (Schwab et al., 1984 and Bedford and Schwab, 1991). This modelling system provides hourly wave and current data for the Great Lakes. For the purposes of this chapter, finer resolution is required to gain a better understanding of the dynamics of the Kingston Basin due to its complex features which are not captured with 5 km resolution. Prakash et al. (2007) modelled the circulation of Lake Ontario also using POM with a 2 km resolution. The model was run without flow through the Niagara and St. Lawrence rivers and the results were compared with the GLCFS. They found that flows through the rivers had a small impact on overall lake circulation, and the changes that did occur were small and confined to within 10 km from each river mouth.

Flow distribution and circulation through the Kingston Basin have been described by Tsanis and Murthy (1990), and by Tsanis et al. (1991), who studied the mean currents in the Kingston Basin over the summer months. The basin has been modelled by Paturi et al. (2012; using ELCOM-Estuary and Lake Computer Model), to examine the stratified flows during the summer and fall months, and by Shore (2009; using FVCOM-Finite Volume Coastal Ocean Model), to investigate the circulation and exchange between the Kingston Basin and Lake Ontario. These two studies found that winds commonly induce gyres in the Kingston Basin, and the predominant circulation patterns can reverse under certain wind conditions.

Although the circulation has been investigated in several other studies, the wave field and the influence of waves on circulation through the Kingston Basin have not been investigated in detail, particularly during strong winter storm events. Understanding the wave and current

processes within the basin will allow, for example, numerical modelling of the impact of offshore wind farms on circulation in Lake Ontario (Chapter 4). In regard to offshore wind power, modelling storm events will help identify the maximum impacts of farm development. The focus of this chapter is on developing a modelling system of the Kingston Basin to investigate large storms in combination with field observations.

State-of-the-art wave models solve the spectral action balance equation using source terms that account for wave generation by wind, non-linear (three-wave and four-wave) interactions, which evolve the shape of the wave spectrum (see Booij et al., 1999), and wave energy dissipation (wave breaking, whitecapping, and bottom friction). The wave model Simulating Waves Nearshore (SWAN; Booij et al., 1999) is used in this chapter to simulate the wave field through the Kingston Basin. SWAN has been used in other studies to simulate waves over steep and complex bathymetry. As an example, Gorrell et al. (2010) found that SWAN accurately predicted the propagation of observed gravity waves to the shoreline over complicated nearshore bathymetry that included a steep submarine canyon in California. As a precursor to this chapter, Chapter 2 used SWAN to describe the wave propagation through the Kingston Basin for two storm events. This model was forced by waves specified at an open boundary at the entrance of the Kingston Basin, which proved to represent waves accurately inside the basin.

Delft3D (Lesser et al., 2004) is a 3-Dimensional (3D) hydrodynamic model that can simulate wave-current interactions by coupling the flow module with SWAN. This modelling suite has been used in several studies successfully. Mulligan et al. (2010) modeled waves and currents over a shoal in Nova Scotia and found that, although the model over-predicted the current magnitude, the direction and timing agreed with observations. Elias et al. (2012) effectively simulated the dominant features in the tidal flow, salinity and wave fields of the mouth

of the Columbia River using Delft3D. The model was particularly effective in reproducing the observed vertical and temporal variations in the current structure.

In this chapter, 5 storm events were simulated using two model domains covering Lake Ontario and the Kingston Basin. The purpose of this chapter is to validate the models using measurements during winter storm events, and use the results to further understand the wave and flow fields through the Kingston Basin. Most of the past modelling efforts in Lake Ontario have focused on summer circulation (e.g. Tsanis et al., 1991; Paturi et al., 2011). There is a need to investigate winter circulation and the wave climate within the lake, in order to understand the strongest annual events and therefore the full seasonal cycle. Chapter 4 extends the use of the model to evaluate the impact of an offshore wind farm in the Kingston Basin.

3.2 Methods

3.2.1 Model Description

The SWAN spectral wave model was used to simulate the surface wave conditions within the Kingston Basin. SWAN computes the evolution of random waves and accounts for refraction, as well as wave generation due to wind, dissipation and non-linear wave-wave interactions (Booij et al., 1999). The evolution of the wave field is described by the action balance equation (Equation 3.1), which equates the propagation of wave action density in each dimension balanced by local changes to the wave spectrum:

$$\frac{\partial}{\partial t}N + \frac{\partial}{\partial x}c_x N + \frac{\partial}{\partial y}c_y N + \frac{\partial}{\partial \sigma}c_\sigma N + \frac{\partial}{\partial \theta}c_\theta N = \frac{S_{tot}}{\sigma} \qquad [3.1]$$

where t is time (s), c_x and c_y are wave celerities in the x and y directions (m s^{-1}), c_θ and c_σ are rates of change of group velocity (speed at which wave action is transported), which describe the directional (θ) rate of turning and frequency (σ) shifting due to changes in currents and water

depth. N is wave action density and S_{tot} are the energy density source terms which describe local changes to the wave spectrum. The energy density source terms include generation by wind, dissipation (whitecapping, bottom friction and depth-induced breaking) and nonlinear interactions (triads and quadruplets).

Delft3D computes the non-steady flow and transport equations that result from meteorological and wave forcing (Deltares, 2011). The Fredsøe formulation was used to represent the stresses due to waves, using the default parameterisation coefficients developed by Soulsby et al. (1993). The Chézy bottom roughness formula was applied using the default coefficient of 65.0 $m^{1/2}$ s^{-1}. The model was implemented as a 2-Dimensional (2D) depth-averaged model. The 2D horizontal momentum equations derived from the Reynolds-averaged Navier-Stokes equations with a Boussinesq approximation and the depth averaged continuity equation are given by:

$$\frac{\partial U}{\partial t} + U\frac{\partial U}{\partial x} + V\frac{\partial U}{\partial y} + \frac{\omega}{h}\frac{\partial U}{\partial \sigma} - fV = -\left(g\frac{\partial \zeta}{\partial x} + g\frac{h}{\rho_0}\int_\sigma^0\left(\frac{\partial \rho}{\partial x} + \frac{\partial \sigma'}{\partial x}\frac{\partial \rho}{\partial \sigma'}\right)\partial\sigma'\right) + \upsilon_H\left(\frac{\partial^2 U}{\partial x^2} + \frac{\partial^2 U}{\partial y^2}\right) + M_x \quad [3.2]$$

$$\frac{\partial V}{\partial t} + U\frac{\partial V}{\partial x} + V\frac{\partial V}{\partial y} + \frac{\omega}{h}\frac{\partial V}{\partial \sigma} + fU = -\left(g\frac{\partial \zeta}{\partial y} + g\frac{h}{\rho_0}\int_\sigma^0\left(\frac{\partial \rho}{\partial y} + \frac{\partial \sigma'}{\partial y}\frac{\partial \rho}{\partial \sigma'}\right)\partial\sigma'\right) + \upsilon_H\left(\frac{\partial^2 V}{\partial x^2} + \frac{\partial^2 V}{\partial y^2}\right) + M_y \quad [3.3]$$

$$\frac{\partial \zeta}{\partial t} + \frac{\partial (hU)}{\partial x} + \frac{\partial (hV)}{\partial y} = 0 \quad [3.4]$$

where U and V are the depth-averaged generalized Lagrangian mean velocity components (m s^{-1}) including waves (Stokes drift components), f is the Coriolis coefficient (s^{-1}), g is gravitational acceleration (m s^{-2}), h is water depth (m), υ_H is the horizontal eddy viscosity (m^2 s^{-1}), ρ is the fluid density (kg m^{-3}), ρ_0 is the reference density of water (kg m^{-3}), σ is the vertical topography following coordinate (m), ζ is the water surface elevation above reference datum (m) and ω is the vertical velocity component in the sigma coordinate system (s^{-1}). M_x and M_y represent

contributions from external sources and sinks of momentum (m s^{-2}) and in this case represent the wave stress terms from SWAN. Wave breaking is modelled as a shear stress at the water surface (Svendsen, 1985; Stive and Wind, 1986) and is simplified using the expression derived by Dingemans et al. (1987).

Two domains were used and compared in this chapter, each using different boundary or input forcing. The Lake Ontario model-domain (LOM, Figure 3.1a), used winds from the GLCFS in the Main Basin of Lake Ontario applied uniformly across the lake, representing typical winter storm conditions (Pickett, 1980). A closed boundary was implemented at the St. Lawrence River as circulation exchange due to the outflow at this boundary is negligible within 10 km of the river (Prakash et al., 2007). The Kingston Basin model-domain (KBM) was used as both a stand-alone domain and as a nested sub-domain of the LOM (Figure 3.1b). The simulations were forced with wind and wave data from the GLCFS and hourly water level data from L1 (Oswego, NY) and L2 (Alexandria Bay, NY) and compared with wave observations within the Kingston Basin and along the Duck-Galloo Ridge. The wave parameters simulated by the GLCFS at site D (Figure 3.2), the location of the Environment Canada Prince Edward Pt. buoy (not deployed in the winter months), were implemented along the southern boundary. This buoy is used to verify the GLCFS during the summer months, insuring an accurate forecast during the winter months for use in this chapter. Water level observations at the southern boundary (from L1 in Figure 3.1a) and at the St. Lawrence River boundary (from L2 in Figure 3.1a) were used to force the KBM hydrodynamic model (NOAA, 2013).

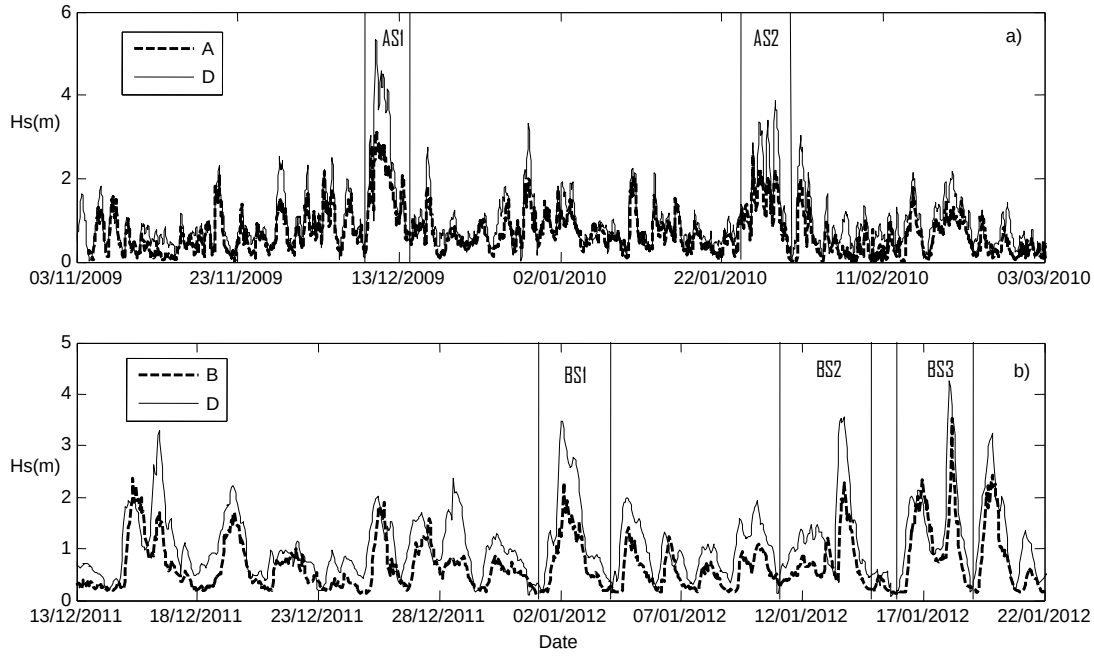

Figure 3.2: Time series of significant wave height (H_s) for two winter periods (a, 2009-10 and b, 2011-12) at various locations (sites A, B, and D). The two storms which will be the focus of this chapter are AS1 and BS1.

3.2.2 Observations

Two sets of observations for waves and currents (outside and inside the Kingston Basin during winter periods in 2009-10 and in 2011-12) were used for model validation. The 2009-10 winter observations were collected using a Nortek AWAC (acoustic wave and current profiler, Figure 3.1b, site A); which captured two significant storm events (Figure 3.2, AS1 and AS2) with H_s up to 3 m and 2 m inside the basin, respectively (H_s outside the basin reached 5.0 m and 3.9 m, respectively). These two events were simulated to ensure accurate representation of the waves and currents at Duck-Galloo Ridge. The 2011-12 winter observations were made with an RDI ADCP (acoustic Doppler current profiler, site B), and RBR TGR and TWR (pressure sensors) deployed by Environment Canada (at sites B and C, respectively). During this period a meteorological station was located at Nine Mile Point on Simcoe Island (site M), providing wind

observations during the 2011-12 winter storms (Figure 2, BS1, BS2 and BS3). These events (BS1-3), with H_s up to 2 m, 2 m and 3.5 m, respectively, (H_s outside the basin reached 3.5 m, 3.5 m and 4.1 m, respectively).were validated to ensure accurate representation of the waves and currents inside the Kingston Basin. Details regarding the instrumentation used for the purposes of this chapter are provided in Table 3.1 and other sensors that recorded water levels are listed in Table 3.2. The AWAC collected 1024 samples per burst with a burst frequency of 2Hz collected once per hour for waves and every 10 minutes for currents, and the ADCP collected 1200 samples per burst with a burst frequency of 2Hz collected hourly.

Table 3.1: Wave and Flow Measuring Instruments near the Kingston Basin

Site	Instrument	h(m)
A	Nortek AWAC (1.2 MHz), 2009-10	18
B	RDI ADCP (600 kHz) & RBR TGR, 2011-12	26
C	RBR TWR (4 Hz), 2011-12	42
D	Buoy 45135 (NOAA GLCFS forecast data)	68
M	Meteorological Station	N/A

Table 3.2: Hourly Water Level Measurement Locations

Site	Location
L1	Oswego, NY
L2	Alexandria Bay, NY
L3	Kingston, ON
L4	Cape Vincent, NY

3.2.3 Model Simulations

3.2.3.1 Lake Ontario Model Domain (LOM)

A spherical orthogonal grid was used for each domain. The LOM consisted of a coarse (3 km) resolution lake wide domain combined with a finer (380 m x 270 m) resolution domain of the Kingston Basin. The internal boundary uses domain decomposition, a 2-way nesting method for connecting the coarser grid (main basin of Lake Ontario) to the finer grid (Kingston Basin).

The combination of these domains makes up the LOM. Simulations were set up with online coupling, meaning the SWAN model has a dynamic interaction with the hydrodynamic model (Deltares, 2011). Each grid cell of the KBM sub-domain was approximately 380 m (north-south) and 270 m (east-west) in size, with the model domain corresponding to approximately 94 km in the longitudinal direction and 63 km in the latitudinal direction. Each grid was created using the bathymetry data of the lake from two sources. The Lake Ontario bathymetry was provided by NOAA (2013) and the bathymetry of the headwaters of the St. Lawrence River, from bathymetric soundings of Environment Canada as described in Paturi et al. (2012). The simulations were run using a model time step of 1 minute.

Waves for the LOM are generated using GLCFS wind data from the main basin of the lake uniformly over the model domain. Wind forcing from observations made inside the basin yielded weaker simulated flow than the observations. Stronger winds from the GLCFS outside the basin yielded better model results. An error analysis of winds from the GLCFS at three locations across the lake was performed and it was determined that the winter storm winds were nearly uniform across the entire domain. Local wind observations at site M were only available during the 2011-12 winter period and therefore, the ability to use GLCFS wind forcing uniformly across the domain allowed for a consistent wind input to the model for all events. Figure 3.3 shows the winds over three areas of the lake during storm AS1. The results of the error analysis indicate an averaged correlation coefficient (R) value of 0.80 and a root-mean-squared error (RMSE) of 2.79 m s^{-1} for wind speed and an averaged R value of 0.95 and RMSE of 20.37° for wind direction. Due to the low spatial variability of the wind conditions, the nearest GLCFS point to the Kingston Basin of the three locations was used to force the LOM. Wind directions from the GLCFS also compared well with observations from the meteorological station (site M) for storms BS1-3.

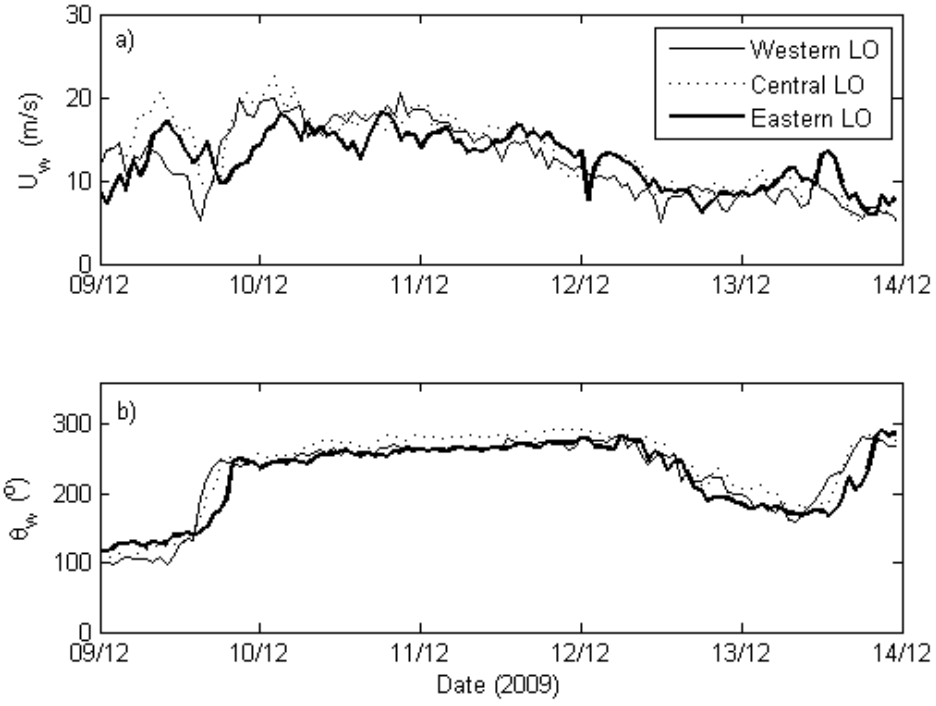

Figure 3.3: Storm AS1 wind magnitude (U_w) and direction (θ_u) for winds at three locations across the longest fetch in the center of Lake Ontario taken from the GLCFS input data (NOAA, 2013).

3.2.3.2 Kingston Basin Model Domain (KBM)

The KBM was forced with parametric wave input (significant wave height, H_s, peak wave period, T_p, wave direction, θ_p, Figure 3.4) from the GLCFS at the Prince Edward Pt. Buoy (site D) along the open boundary shown in Figure 3.1 at latitude 43.8^o N, and wind hindcast results (wind magnitude, U_w, and direction) from the GLCFS. The wind and wave inputs for the two storms (AS1 and BS1), are shown in Figure 3.4. Strong northwesterly winds exceeding 14 m s^{-1} produced waves with a significant wave height over 5 m (during AS1) at the southern boundary of the model domain. Wind data was spatially uniform over the spherical grid and was obtained from the GLCFS for AS1 and from the meteorological observations (Figure 3.1b, site M) for BS1.

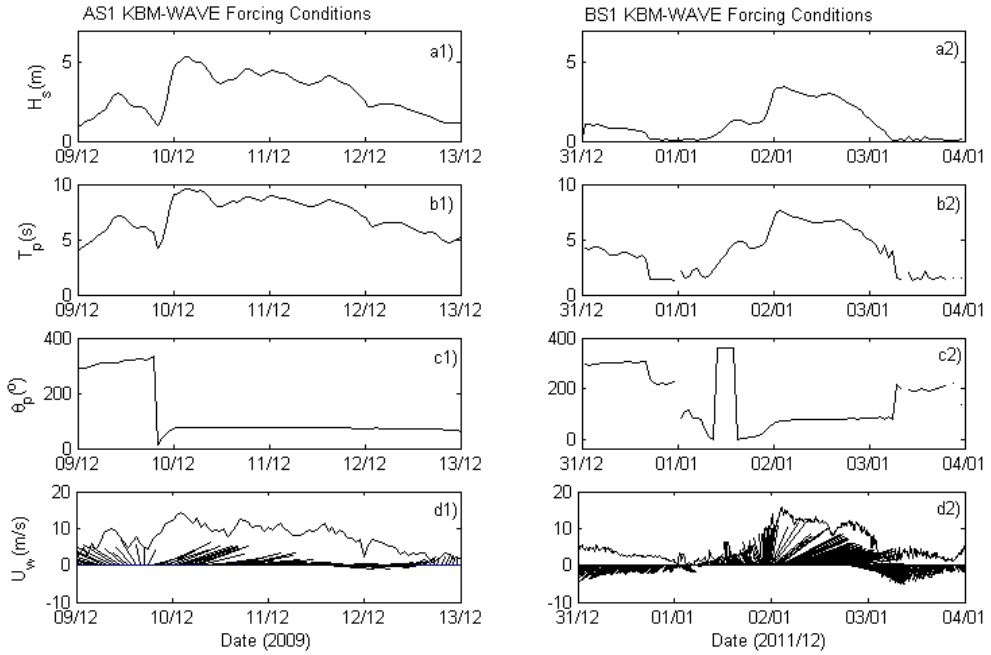

Figure 3.4: Storm AS1(1) and BS1(2) significant wave height (H_s, a), wave period (T_p, b), wave direction (θ_p, c) and wind speed and wind direction vector (U_w, d) wave forcing conditions for the KBM.

Circulation in the KBM was simulated using hourly water level data from L1, as it is the nearest point to the southern boundary of the model, which may accurately represent changes in water levels along the boundary of the model grid. Water levels measured at L2 were used to force an outflow at the St. Lawrence River Boundary. Model forcing conditions for the LOM and the KBM are provided in Figure 3.5. The storm surge during AS1 was a maximum of approximately 0.25 m at the southern boundary and was 0.1 m during BS1. A summary of statistical comparisons between the LOM and the KBM is provided in Table 3.3. Table B.1 in Appendix B provides a list of parameters used for model simulation. The results and details of sensitivity analysis performed with changes to horizontal eddy viscosity, the Chézy roughness coefficient and model resolution are provided in Appendix C.

Table 3.3: Statistical Comparison of the LOM and the KBM Averaged Over All Storms

	LOM	**KBM**
Grid Dimensions	3 km x 3 km with 380 m x 270 m K.B. sub-grid	380 m x 270 m
Domain Lengths	125 km x 300 km with 63 km x 94 km sub-grid	63 km x 94 km
RMSE (m) H_s at site A	0.34	0.59
R H_s at site A	0.90	0.89
RMSE (m) H_s at site B	0.50	0.30
R H_s at site B	0.78	0.92
RMSE (m) ζ at site L3	0.05	0.04
RMSE (m) ζ at site L4	0.065	0.06

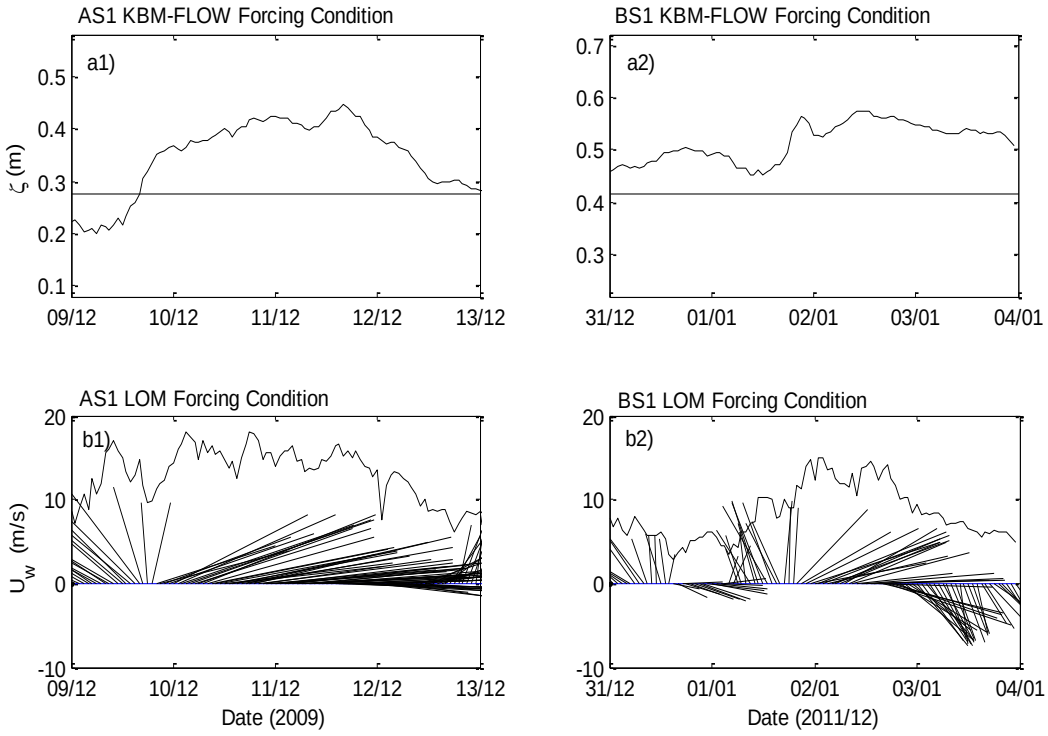

Figure 3.5: Water levels (ζ, a) and wind magnitude and direction vectors (U_w, b) forcing, driving currents through the model. Input for AS1 located on the left (1) and BS1 on the right (2). Note that the average water level for each month is provided (NOAA, 2013) as a horizontal reference line.

3.3 Results

3.3.1 Model Verification

3.3.1.1 Waves

The wave model was validated by minimizing errors in significant wave height and period between observations and model results. The model-data comparison in Figure 3.6 indicates that the LOM simulations reproduce the significant wave height accurately with slight over-predictions (< 0.4 m) at storm peaks (Figure 3.6, a1 and b1). To quantify the accuracy of each simulation for each of the five storms, scatter plots (Figure 3.7) and the correlation coefficients (R) between simulated and observed H_s time series were computed. Average root mean squared errors (RMSE) and average R values at site A were 0.34 m and 0.90, respectively, and for site B, 0.50 m and 0.78. The waves outside of the Kingston Basin (site A) are better represented than those inside the basin by the model. A higher resolution domain capturing the smaller islands and resolving the shape of large islands might reduce this error in the future.

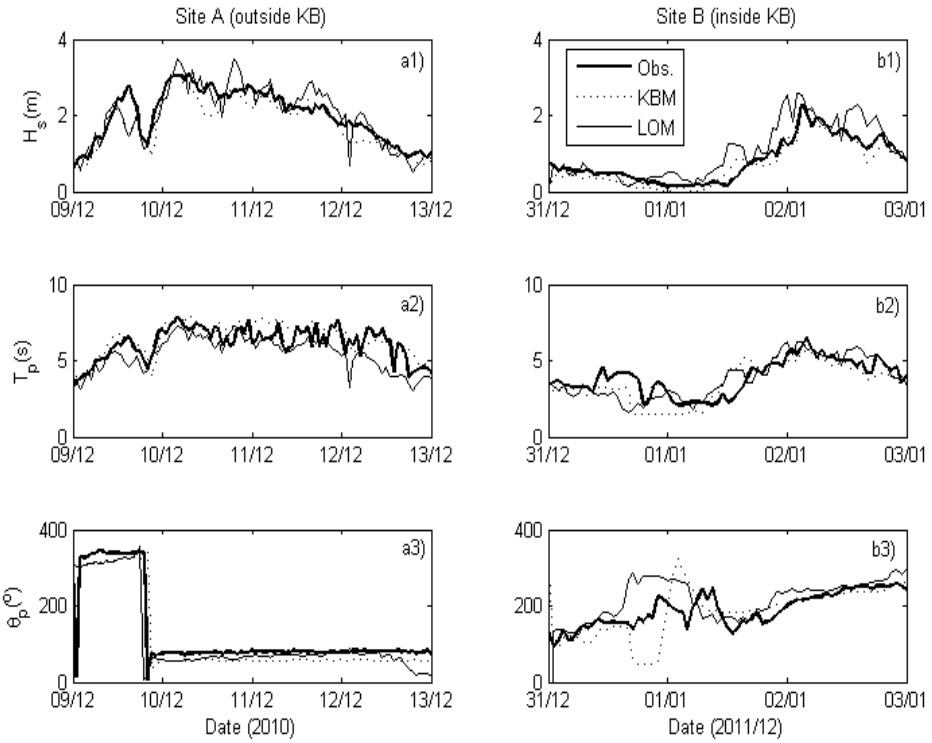

Figure 3.6: Wave simulation comparisons with observations from site A for storm AS1 (a) and from site B for storm BS1 (b) of various wave parameters: 1) Significant Wave Height (H_s), 2) Wave Period (T_p) and 3) Wave Direction (θ_p). AWAC and ADCP data shown were averaged hourly.

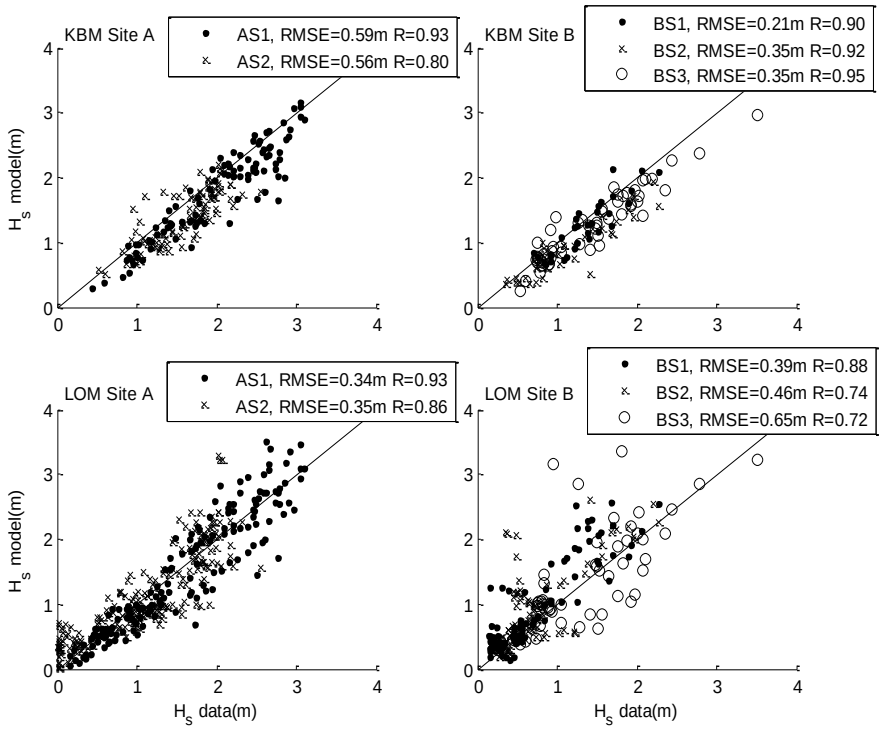

Figure 3.7: Scatterplots of significant wave height (H_s) from observations (H_s data) and model predictions (H_s model) at sites A and B.

Spectral energy comparisons to observations indicate that the total energy of waves is well represented. The observed (*Obs*) and simulated wave spectra (*LOM*) are compared for different times at site A (outside the basin) and site B (inside the basin), in Figure 3.8. The primary peak in the wave spectrum and energy level of these peaks between 0.1 and 0.2Hz as well as secondary peaks are reproduced by the model.

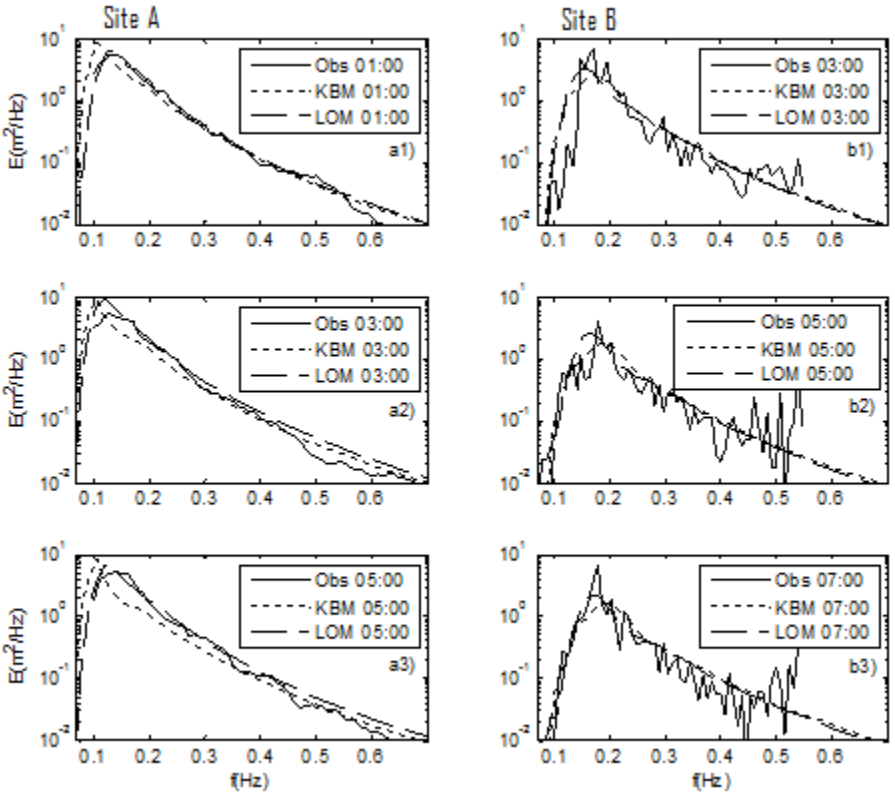

Figure 3.8: Comparison of surface elevation spectra for observations from the ADCP and AWAC (Obs Site A and Obs Site B, respectively) and SWAN (coupled with Delft3D) simulations at different times of storms AS1 (a) and BS1 (b) at storm peaks (2), four hours prior to strom peaks (1) and four hours after storm peaks (3). Peak for AS1 occurs 10/12/2009 and for BS1, 02/01/2012.

3.3.1.2 Currents

Comparisons of the currents were made using AWAC and ADCP measurements at sites A and B, respectively. During each storm event, observations indicate that the currents are near-uniform over the depth (Figure 3.9) which agrees with the findings of Beletsky et al (1999) for mean conditions in winter. Since the currents are uniform over the depth, a barotropic (depth-averaged) model is appropriate to describe the circulation in the basin at this time of year. The velocity observations (Figure 3.10) indicate that for similar storm events, currents outside the

Kingston Basin (site A) are much faster compared to inside the basin (site B). Flows are weakened (up to 0.11 m s^{-1}) due to the momentum loss over the ridge. The model generally under-predicted the flow through the Kingston Basin. The RMSE of flow in the LOM, when compared to observations, was 0.08 m s^{-1} and 0.05 m s^{-1} for AS1 and BS1, respectively.

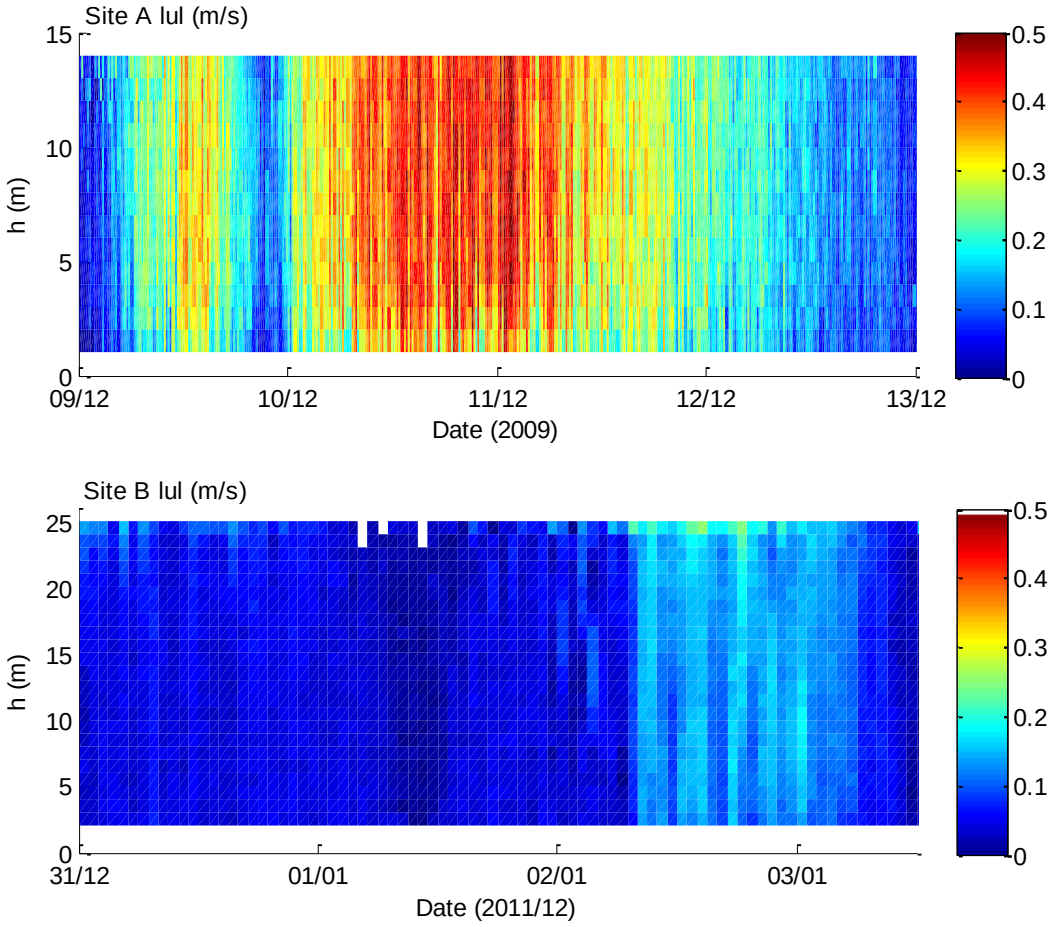

Figure 3.9: AWAC and ADCP (site A and B) horizontal velocity profile magnitude observations, for AS1 and BS1, respectively, binned every meter where *h* is the height above the bottom. The AWAC data was averaged every 15 minutes (water depth 18 m) and ADCP data was averaged hourly (water depth 26 m).

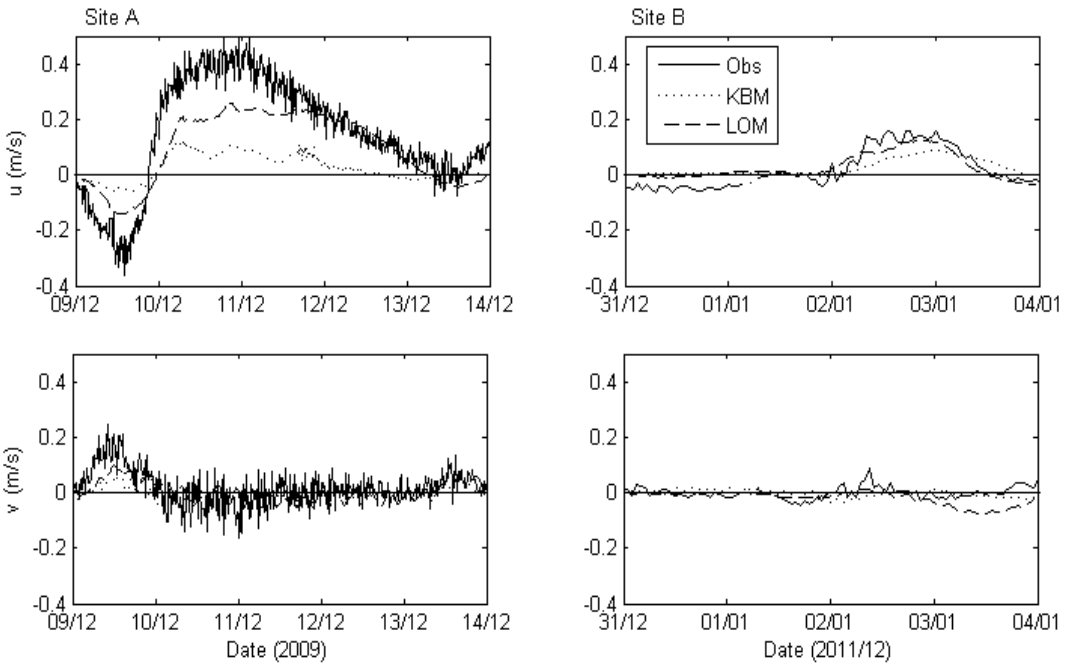

Figure 3.10: Comparison of each component of the horizontal velocity at sites A and B over the course of storms AS1 (left) and BS1 (right).

3.3.1.3 Water Levels

A comparison of water level simulation results to measurements at L3 and L4 is provided in Figure 3.11. The LOM underestimates the storm surge and does not capture the decrease in water level seen in Figure 3.11. These changes in water level may be due to a longer term process which is not accounted for, given the short duration of the simulation (e.g., surface seiching prior to storm event). The average RMSE of water levels is 0.06 m. The mode-one surface seiching period simulated by the model was approximately 5 hours in length, as observed by Hamblin (1982) for the fall months of 1972.

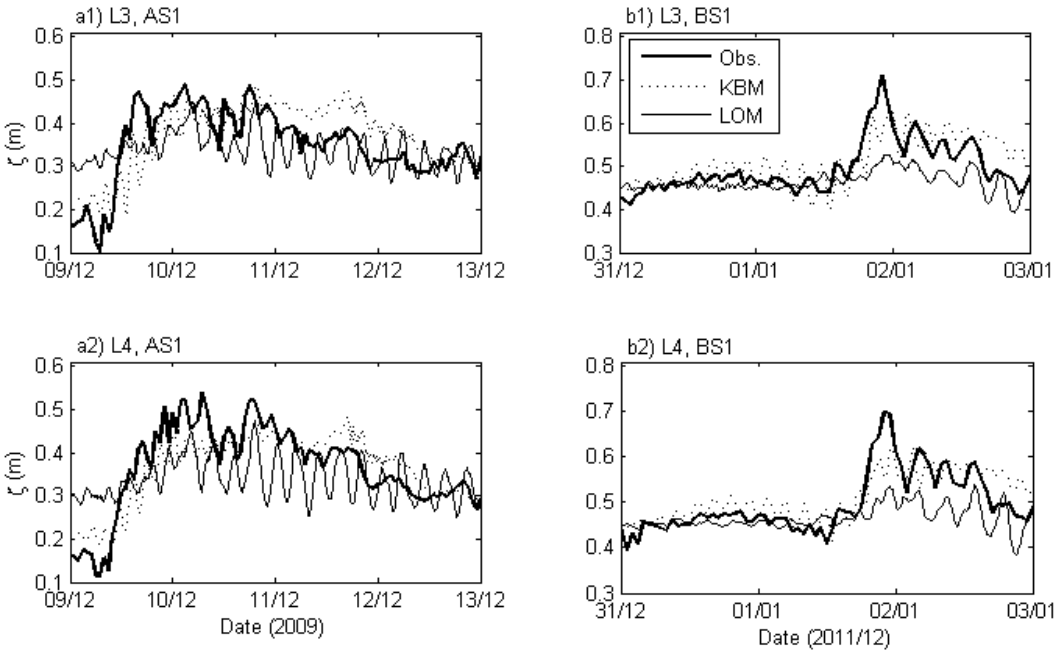

Figure 3.11: Water level (ζ) comparisons of observations at Kingston, ON (L3; 1) and Cape Vincent, NY (L4; 2) to simulation results for storms AS1 (a) and BS1 (b).

3.3.2 Wave Field

The simulated H_s over Lake Ontario in Figure 3.12 (a) illustrates how waves propagate from the Mississauga Basin, to the Rochester Basin and finally into the Kingston Basin at the storm peak. The spectral shapes indicate that one low-frequency (< 0.2 Hz) peak generally occurs in the wave spectrum at site A outside the basin (Figure 3.8, a1-3) and a broader higher-frequency peak (> 0.20 Hz) generally occurs at site B inside the basin (Figure 3.8, b1-3). The first peak in the spectrum for sites A and B is < 0.2 Hz and corresponds to lower frequency swell moving into and throughout the Kingston Basin from the main basin of the lake. The second peak, > 0.2 Hz, represents a higher frequency transient wind-sea peak from wave growth within the Kingston Basin. The wave directions at the peak of AS1 are shown in Figure 3.13 (b) using wave direction vectors, to illustrate the effect of the Duck-Galloo Ridge on the wave field. The ridge causes

wave energy to refract into the two channels on either side of Main Duck Island. Wave energy is dissipated as waves break over and is spread out as waves refract around the islands spanning the ridge. As shown by Figure 3.13 (b), the wave height reduces as waves pass over the ridge and refract throughout the model domain. This may be particularly important in the center of the basin where a wind farm has been proposed (Ortech Environmental, 2010), the influence of which is investigated in chapter 4.

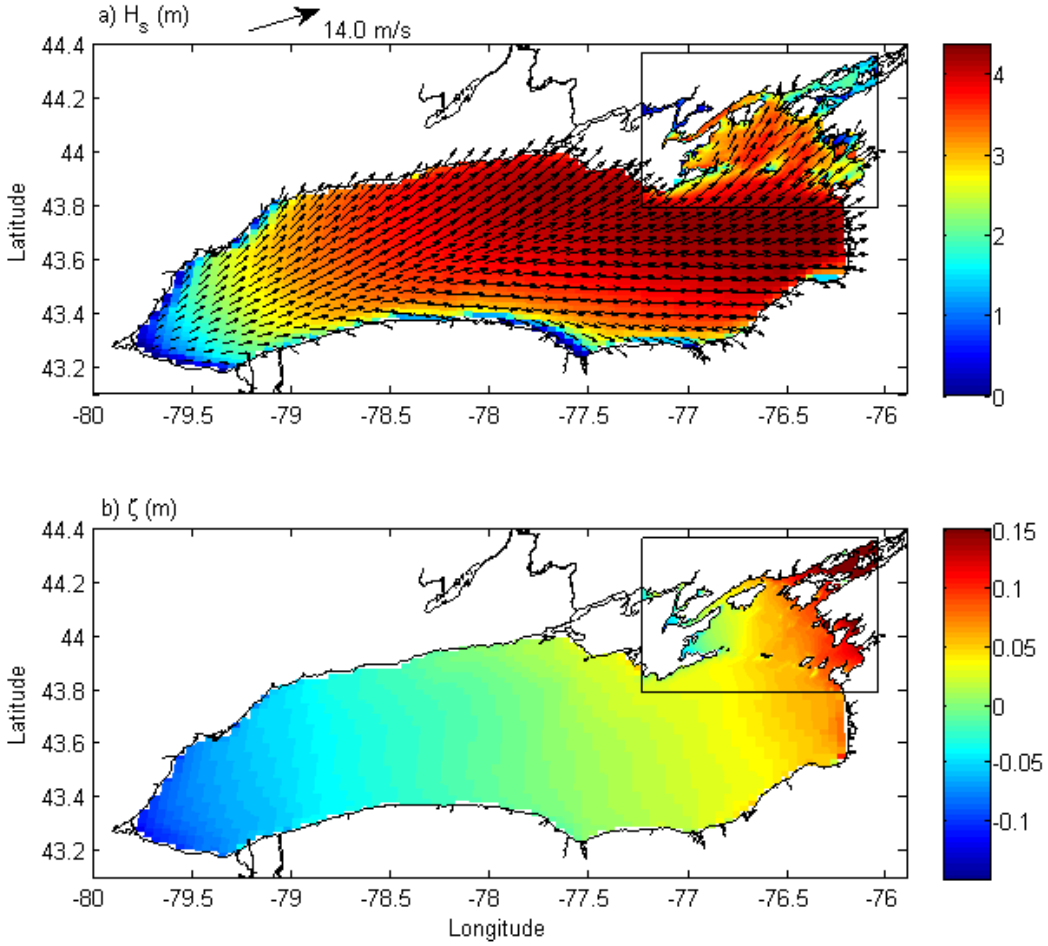

Figure 3.12: Significant wave height (H_s) and water level (ζ) predicted for AS1 at 18/01/2012, 03:00.

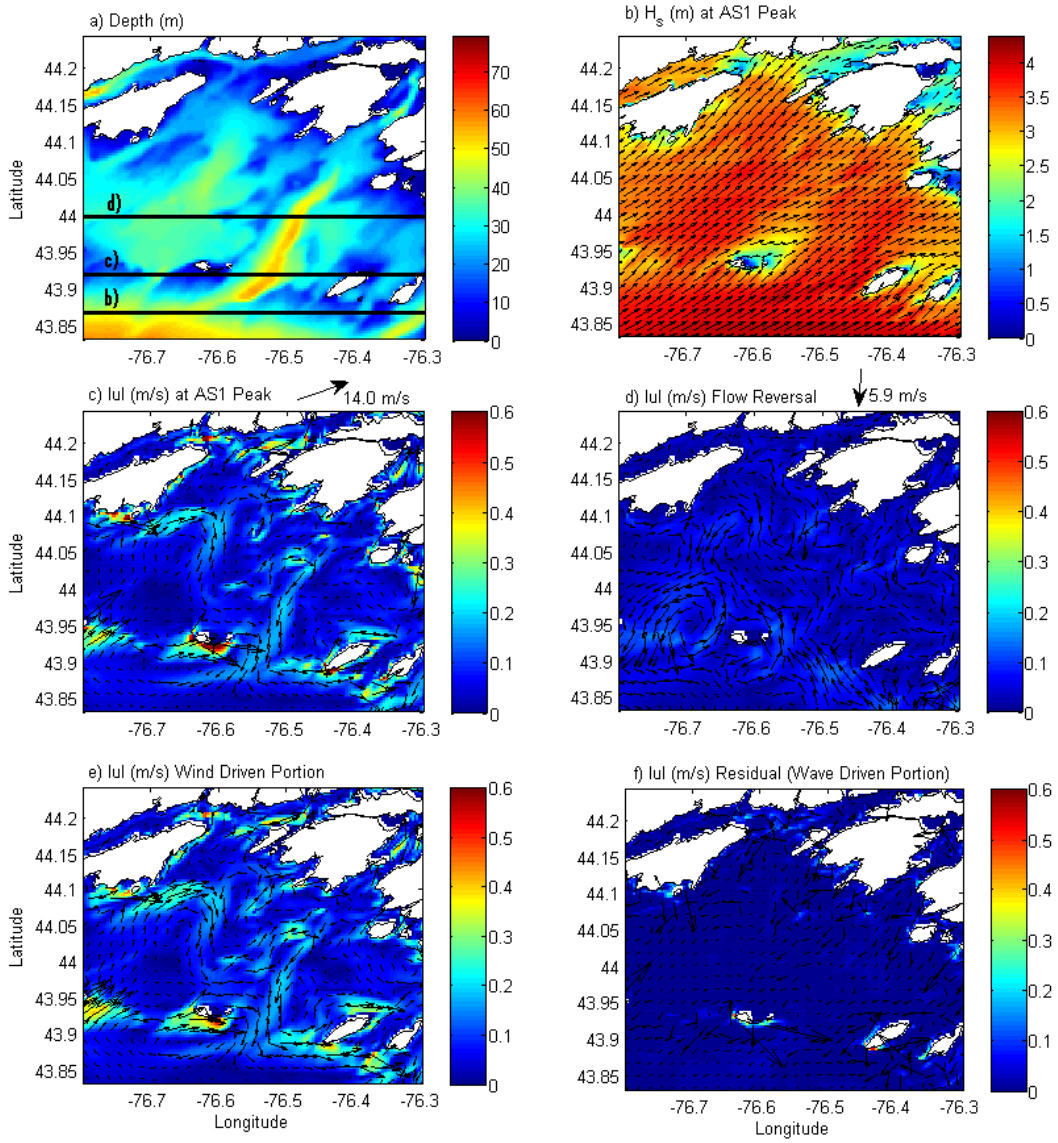

Figure 3.13: a) Bathymetry of the Kingston Basin with cross sections b, c, and d used in Figure 3.14 shown (cross-section (a) is at the southern boundary of the KBM). b) Significant wave height (H_s) and wave direction vectors, whose lengths indicate H_s magnitude, at the peak of storm AS1 (18/01/2012, 03:00). c) Current magnitude ($|u|$) and direction vectors during the peak of AS1 with wind direction and speed shown. d) Example of flow reversal occurring during easterly wind conditions as shown. e) Delft3D simulation at the peak of storm AS1 where the SWAN wave model is not implemented. d) The residual of the coupled model and the flow only model representing the impact of waves on the currents in the Kingston Basin.

To help understand the wave propagation from the main basin of the lake, across the Duck-Galloo Ridge, and into the Kingston Basin, depth and wave energy density contours along four longitudinal cross-sections were constructed (Figure 3.14, locations shown in Figure 3.13). The wave energy (E) which passes over the Duck-Galloo Ridge and into the two channels on each side of Main Duck Island was determined using (e.g. Kamphuis, 2010):

$$E = 1/8\ \rho g {H_s}^2 \qquad [3.5]$$

where ρ is the density of fresh water (kg m^{-3}), g the acceleration due to gravity (m s^{-2}) and H_s the significant wave height (m). As waves propagate into and throughout the Kingston Basin, a reduction in energy density occurs approaching the Duck-Galloo Ridge (Figure 3.14, b). Once waves reach the ridge, the energy density is reduced even further as energy is lost due to wave breaking (Figure 3.14, c). Two of the islands (Main Duck Island and Galloo Island) can be identified where the energy density approaches zero. The influence of the two islands on the energy density of waves within the basin is less apparent as waves propagate into the Kingston Basin (Figures 3.14, d) and shorter period waves are generated by local winds. The largest waves entering the basin lose approximately 18-19% of their incident wave energy density due to the influence of the Duck-Galloo Ridge. Energy density continues to diminish as wave energy is lost with the propagation and refraction of waves through the model domain toward the head of the St. Lawrence River. Waves through the Simcoe Island Channel lose approximately 10% of their energy and waves entering through the St. Lawrence Channel lose approximately 6%. The St. Lawrence Channel is the deepest area along the Duck Galloo Ridge where the effect of refraction is minimized.

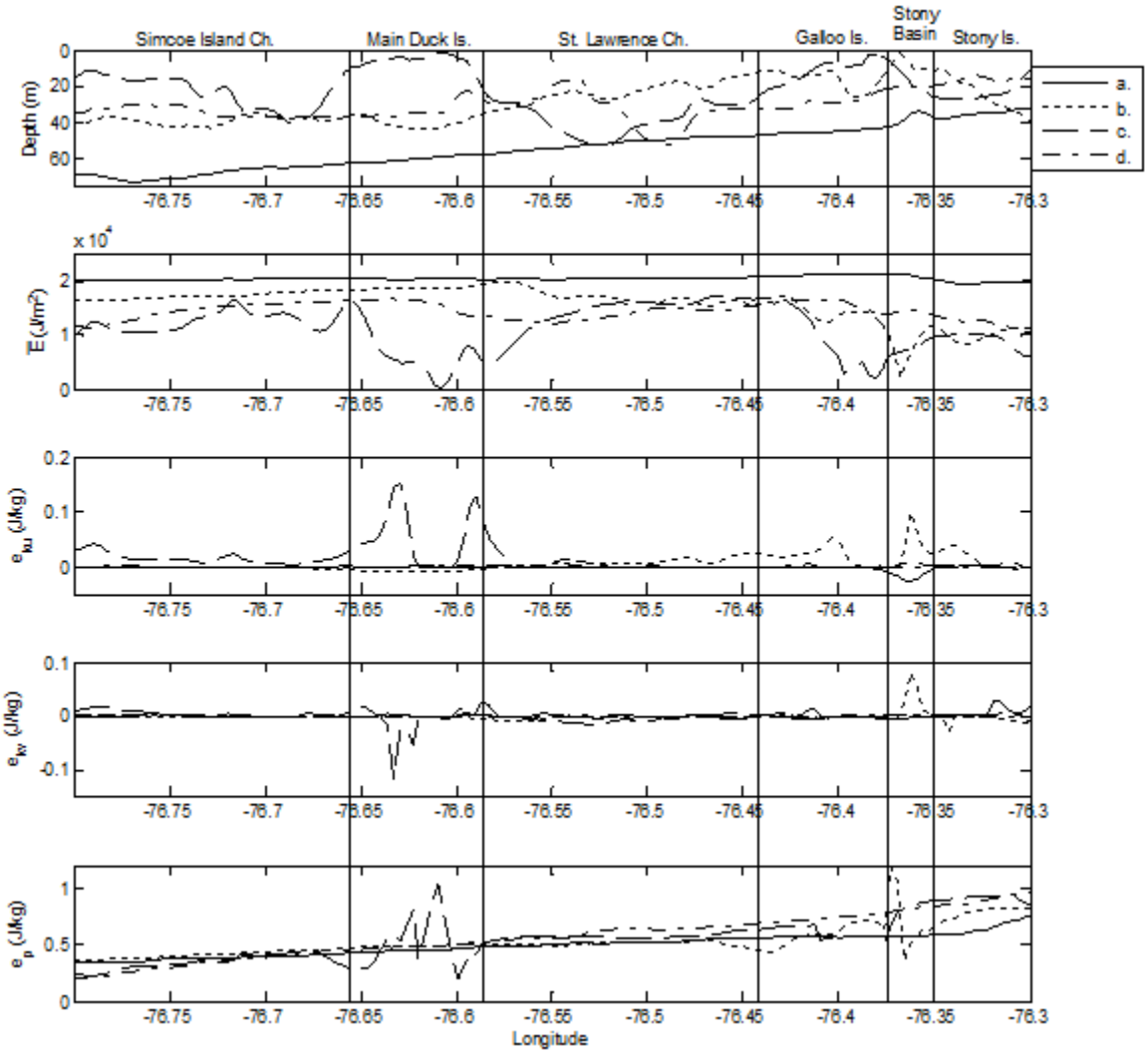

Figure 3.14: Water depth, wave energy density ($\bar{E}$), kinetic energy per unit mass in the u and v directions (e_{ku} and e_{kv}) and potential energy per unit mass (e_p) through the cross-sections of the Kingston Basin shown in Figure 3.13 (the straight line (a) represents the southern boundary of the KBM).

3.3.3 Flow Field

Figure 3.13 illustrates examples of the wind induced circulation features predicted by the LOM inside the Kingston Basin. The double gyres (as discussed by Shore 2009 and Bennet 1974) in the main basin of the lake and rotating in opposing directions are reproduced by the model. Some of this flow crosses the Duck-Galloo Ridge through the Simcoe Island Channel and the

small channels to the east of Galloo Island (Figure 3.13, c). The currents, which are generated in the Kingston Basin, form a more coherent gyre near Amherst Island and other complex smaller-scale flow patterns further inside the basin. A plot showing the same time step with the wave portion of the model removed shows a relatively unchanged flow field in the Kingston Basin (Figure 3.13, e). The residual of the coupled model to the flow-only model suggests that wave impact on flows occurs mainly where waves break near islands and along the shoreline, indicating that currents are mostly wind induced in deeper areas. Waves have minimal impact on the general circulation pattern in the deep areas, although they dominate across the shallowest shoals and along coastlines. Figure 3.13 (d) shows a flow reversal in the basin when a weak north-easterly wind forces opposite flow conditions in the domain. At this time, the flows in the St. Lawrence River are < 0.03 m s^{-1}.

The kinetic and potential energy through the same four cross-sections used to describe waves, were computed to gain a better understanding of currents (Figure 3.14). The kinetic energy per unit mass (e_{ku}, e_{kv}) and potential energy per unit mass (e_p) were determined using:

$$e_{ku} = \frac{1}{2}u|u|, \; e_{kv} = \frac{1}{2}v|v| \qquad [3.6, 3.7]$$

$$e_p = g\zeta \qquad [3.8]$$

where u and v are the longitudinal and latitudinal components of depth averaged velocity (m s^{-1}), respectively, g is gravitational acceleration (m s^{-2}) and ζ is water level (m). Kinetic energy south of the islands along the Duck-Galloo Ridge flows to the east on the western-most end of the Simcoe Island Channel and to the south in the St. Lawrence Channel out of the Kingston Basin. There also exists a strong flow into the basin at the east of Galloo Island. The potential energy (Figure 3.14) indicates a gradient from west to east, which represents the storm surge at the east

end of the lake. The extent of the gradient (across the lake) can be seen in terms of water level in Figure 3.12 (b).

3.4 Discussion and Conclusions

Overall, the circulation patterns inside the basin match qualitatively with past studies for summer and the present study extends the previous works for stronger winter storm events and includes the effects of waves. The double gyre circulation in the main basin of Lake Ontario (Shore, 2009; Bennet, 1974) is reproduced by Delft3D in the Lake Ontario domain during the storm simulations. The closed nature of Lake Ontario under uniform wind conditions forces flows in the coastal regions downwind (to the east). To compensate, a return circulation in the middle of the lake is produced. This process was first discovered using a numerical model by Rao and Murty (1970) and has since been reproduced and observed in many studies (e.g. Beletsky et al., 1999; Rueda and Vidal, 2009). The gyres forming inside the Kingston Basin (Figure 3.13) have also been modelled by both Paturi et al. (2012) and Shore (2009), who found a strong cyclonic gyre between Amherst Island and Wolfe Island in the western portion of the Kingston Basin, which is also reproduced by Delft3D in this chapter. The complex circulation inside the basin could be caused by shoreline irregularities (Rueda and Vidal, 2009) since sharp bathymetric features and large velocity gradients, such as those found in the Kingston Basin, can generally cause gyres to form. Additionally, inflow to the Kingston Basin from the Rochester Basin of the lake occurs at the west and east ends of the lake as a result of the double gyre formed in the main basin while an outflow occurs through the Duck-Galloo Ridge at the St. Lawrence Channel. The circulation within the basin is highly complex with smaller gyres forming in generally opposing directions, which are magnified during storm events.

The flow in the Simcoe Island Channel (41.2 m deep) during peak storm conditions were low (0.02-0.04 m s^{-1}) and directed into the basin, while flows in the St. Lawrence Channel (56.2 m deep) exhibited much stronger outflows of up to 0.2 m s^{-1} from the Kingston Basin. Paturi et al. (2012) identified flow reversal in the St. Lawrence River with easterly winds of approximately 10 m s^{-1} during a simulation of a period of approximately 6 months. In this chapter, flow reversal throughout the Kingston Basin occurs at slightly lower wind speeds (~6 m s^{-1}), when flow reversal in the St. Lawrence River is not apparent.

At the peak of significant wave height for storm events AS1 and BS1, it was determined that waves propagating from the main basin into the Kingston Basin, using the LOM, lose approximately 18-19% of their energy density due to breaking and refraction over Duck-Galloo Ridge. Outside the basin, waves with significant wave heights of up to 5 m and periods up to 10 s were observed. Within the basin, waves are composed of both swell and wind-sea spectral components resulting in significant wave heights up to approximately 3.5 m and peak wave periods up to 7 s. During the largest storms identified, wave directions were near-perpendicular to the Ridge, causing swell to refract and enter the basin through the Simcoe Island and St. Lawrence Channels surrounding Main Duck Island. The impact of waves on the circulation patterns at the basin scale are negligible, since shoals are typically too deep (e.g. 20m) relative to the wavelength and period (e.g. 7-10 s) to generate large-scale wave-driven flows.

Two model domains were used for simulation, including the entire Lake Ontario model domain (LOM) which used a nested finer grid of Kingston Basin, and a stand-alone Kingston Basin model domain (KBM). Overall, the KBM provided a slightly better representation of the waves, which was expected since it was forced by local winds and wave boundary conditions, whereas the LOM wind forcing conditions were applied uniformly across the entire lake. The

KBM provides an overall better representation of waves when compared to the LOM, but the frequencies at which these spectral peaks occur are better represented by the LOM. This suggests that, although significant wave heights and wave periods may be more accurately represented by the KBM, the wave energy entering the Kingston Basin is better represented as a spatially varying forcing condition along the southern boundary of the model domain (LOM). The LOM was able to better capture the magnitude and direction of the currents during each storm event than the KBM. The LOM was 44% more accurate than the KBM for AS1 and, 24% more accurate for BS1. The complexity of the circulation at the boundary in the KBM is not captured, since it was forced with a spatially uniform boundary condition. The LOM allows for the full circulation pattern of the lake to develop and provide a better input to the KBM sub-domain. The KBM water level results are slightly more accurate with an average RMSE of 0.05 m as can be expected as water levels from Oswego were directly input into the model space at the southern boundary.

Understanding the surface wave and circulation in the Kingston Basin during major winter storm events will help to determine if the changes in waves and flow patterns due to offshore wind farm construction within the Kingston Basin would impact the surrounding areas, and may be applicable to future offshore wind farm consideration within the Great Lakes. The storms modelled in this chapter are accurately reproduced and it is recommended that the LOM model be applied to simulate offshore wind farm impacts in the Kingston Basin (see Chapter 4).

Chapter 4

Offshore Wind Farm Impacts on Surface Waves and Circulation in Eastern Lake Ontario

4.1 Introduction

The Ontario government imposed a moratorium on constructing offshore wind farms in the Great Lakes in August, 2011, declaring that further scientific research on impacts to the lakes is required. Although many offshore wind projects have been carried out and studied in coastal areas in Europe (e.g. Scroby Sands; CEFAS, 2006, Horn Rev and Nysted; Danish Energy Autority, 2006), wind farm impacts on freshwater systems are less well understood. An example of a small operational farm is in Lake Vanern in Sweden, although the scale of the lake (5,655 km^2) and the farm (10 turbines) is small compared to what has been proposed for Lake Ontario (18,960 km^2, 130 turbines; Ortech Environmental, 2010), shown in Figure 4.1. Scientific and technical issues associated with potential offshore wind farm development in North America have been studied (Baird, 2011; Manwell et al., 2007), highlighting the issues (e.g., freshwater ice, social and ecological impacts, etc.) to consider for Great Lakes wind farms. Literature regarding offshore wind farm impacts in the Great Lakes is limited and there is a need for research in this area.

The purpose of this chapter is to model and understand the near and far-field effects of an offshore wind farm on the waves and circulation through eastern Lake Ontario (Figure 4.1a) known as the Kingston Basin (Figure 4.1b), where we define near-field as the area within the wind farm and 1 km outside the turbines, and far-field as the area more than 1 km away from the turbines. The simulated wind farm is between Wolfe Island and Main Duck Island shown in

Figure 4.1b. The area of the wind farm is constrained by the USA/Canada border, the water depth (< 30 m) and the distance from the coastline (minimum 5 km). A model of Lake Ontario, with a higher-resolution nested grid of Kingston Basin, has been described in Chapter 3 and a similar version of this modelling system is used in this chapter to simulate the effects of a wind farm that is based on a proposed design by Ortech Environmental (2010). The modelling system uses a hydrodynamic model (Delft3D, Lesser et al., 2004), coupled to a surface wave model (SWAN, Booij et al., 1999) to predict the waves and circulation.

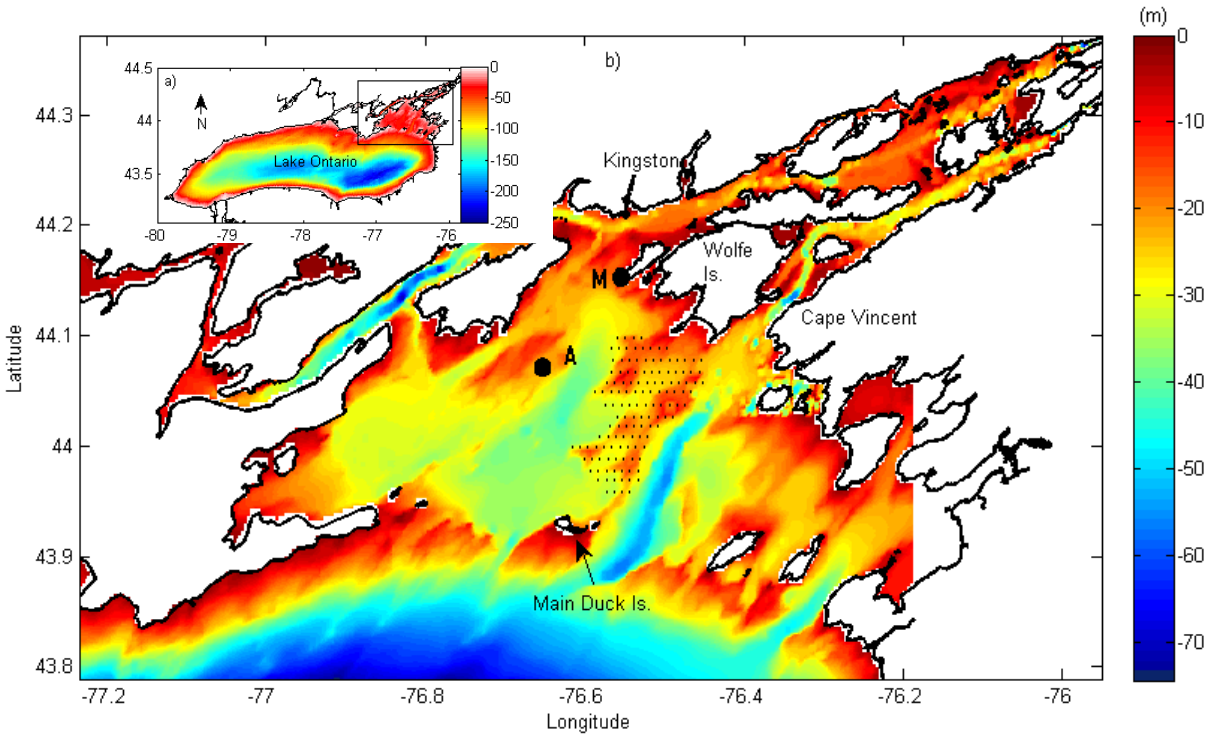

Figure 4.1: Lake Ontario (inset, a) and northeastern Lake Ontario (Kingston Basin, b) with wind farm turbine locations shown on the 20-30 m deep shoal between Wolfe Island and Main Duck Island. The large dot A represents the location of the ADCP and dot M represents the location of the meteorological station deployed during the 2011-12 winter months.

Various methods have been used to represent the impact of offshore wind farms on waves in other studies. Ponce de Léon et al. (2011) used SWAN to simulate waves in an offshore wind

farm on the Norwegian continental shelf. Since the monopile foundations considered in their study could not realistically be reproduced without a high level of computational effort, each monopile foundation was represented within the model domain as a dry point (i.e., land), reducing wave energy. They found that overall, the simulated monopiles acted as obstacles blocking the propagation of wave energy and slightly altering the wave direction. Alari and Raudsepp (2012) also used SWAN to simulate changes in significant wave height due to offshore wind farms in the Baltic Sea. In their study, the wind farms were represented using five nested models with the finest resolution of 25 m. The cells closest to the locations of the turbines were given a depth value of 0 (land value). They concluded that changes to significant wave height were very marginal, at < 1% in the far-field. Other relevant studies (e.g. Cooper and Beiboer, 2002) also suggest that changes to the wave field due to offshore wind farms in various locations, are unlikely to be significant in the far-field and are small in the near-field.

SWAN has the ability to implement sub-grid obstacles into a given domain. The influence of these obstacles is represented by a transmission coefficient. This technique has been used to represent single turbines (e.g. Ponce de Léon et al., 2011) and to represent wind farm arrays (e.g. ETSU, 2002; Millar et al., 2007). This technique is used in this chapter to assess the impacts of an offshore wind farm on the wave-field of the Kingston Basin.

Changes to currents and circulation patterns are also of concern when assessing the impacts of potential offshore wind farms. Wind farm turbine piles may have effects on flows in the far-field, including flow separation and vortex shedding (Sumer and Fredsøe, 1997), and group-effects in the near-field (Sumer and Fredsøe, 2002). ETSU (2002) conducted a study using Delft3D to model 30 turbines in Liverpool Bay, UK, and found that circulation changes were small and that the greatest impacts would be seen in the near-field. Baird (2011) suggested that

currents in the Great Lakes can be expected to change 2-4% in the near-field and < 1% in the far-field based on past studies (e.g. Cooper and Beiboer, 2002; CEFAS, 2006). A quadratic friction term, added to the fluid momentum equations, was used in this chapter to simulate an offshore wind farm and predict the impacts on the flow-field of the Kingston Basin.

4.2 Model Setup

The offshore wind farm was simulated by applying a transmission coefficient in the wave model and adding a quadratic friction term to the momentum equations of the hydrodynamic model, in the area of the proposed wind farm. The proposed wind farm (see Ortech Environmental, 2010) consisted of a total of 130 monopile foundation turbines with a total wind farm area of approximately 130 km^2, which corresponds to 1 km spacing between piles with 7 m diameter piles and an average water depth of 26 m over the wind farm.

The largest winter storm of 2011-12, observed by an ADCP (acoustic Doppler current profiler at site A, Figure 4.1b), was used for model simulation. The storm occurred from January 16-18, 2012, and reached significant wave heights of up to 3.5 m and peak wave periods of 7 s measured by the ADCP at site A (Figure 4.2). The wind forcing applied to the model were observations made by a meteorological station on Simcoe Island (M in Figure 4.1b), measuring wind speed and direction at 10 m, averaged every 10 minutes. Wind and wave directions rotated from south to southwest to west during the storm, which represent the primary wave directions in the Kingston Basin (Figure 4.3).

The correlation coefficient (R) and the root mean squared error (RMSE) of waves, currents and water levels comparing observations to simulated results is provided in Figure 4.3. The model accurately reproduces the conditions of the Kingston Basin.

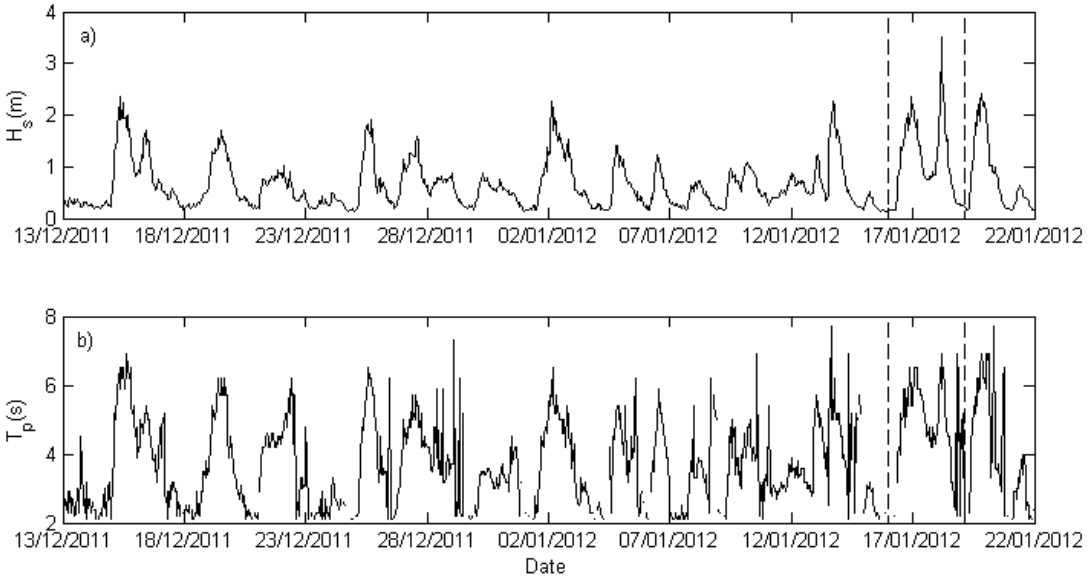

Figure 4.2: Significant wave height (H_s) and peak wave period (T_p) observed at site A over the 2011-12 winter period. Vertical lines indicate the simuation period from 00:00 16/01/2012 to 23:00 18/01/2012. This storm is refered to storm BS3 in Chapters 2 and 3.

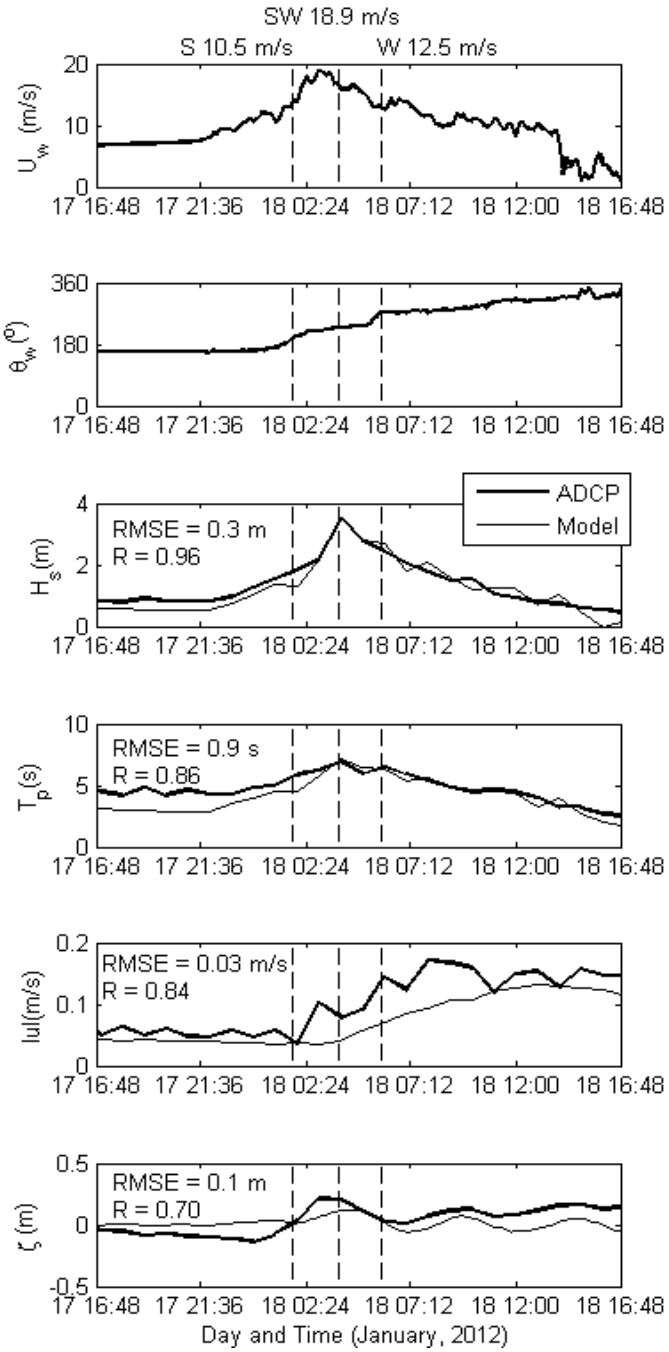

Figure 4.3: Wind forcing velocity (U_w) and direction (θ_w) for the simulated storm, from site M, significant wave height (H_s), peak wave period (T_p), depth averaged velocity ($|u|$) and water level (ζ) comparison of observations at site A and simulated results. Vertical lines indicate the times shown in Figures 4.5 and 4.6.

4.2.1 Transmission Coefficient

To represent the wind turbines as individual piles would demand a much finer resolution model with increased computational effort. To simplify the wind farm, Millar et al. (2005) used a transmission coefficient to efficiently model the bulk effects of a group of turbines. This technique is used in this chapter, and the transmission coefficient in SWAN is based on the following equations by Hayashi et al. (1966):

$$c_t = 4\left(\frac{d}{H_i}\right)E\left[-E+\sqrt{E^2+\frac{H_i}{2d}}\right] \quad , \quad E = C_d\left(\frac{b}{D+b}\right)\Big/\sqrt{1-\left(\frac{b}{D+b}\right)^2} \qquad [4.1, 4.2]$$

where d is depth (m), H_i is incident significant wave height (m), D is the pile diameter (m), b is the pile spacing (m), and C_d is the drag coefficient of the piles (1.0 for a smooth pile). Reflections were not implemented in the simulation as individual piles are not represented. The turbines are represented as straight rows with equidistant spacing (Figure 4.1b).

4.2.2 Energy Loss Due to Turbine Drag

In order to assess the impact of turbines on the circulation throughout the basin, an energy loss term was applied (as in ETSU, 2002);

$$c_{loss\_v} = \frac{NC_dD}{2\Delta x}\left(\frac{A_{tot}}{A_{eff}}\right)^2 \qquad (4.3)$$

where N is the number of piles per grid cell, C_d is the pile drag coefficient, D is the pile diameter (m), Δx is the length of the pile group segment (m), A_{tot} is the total cross-sectional area (m^2) and A_{eff} is the effective wet cross-sectional area (m^2). This energy loss term was applied in parallel rows, similar to those used for the application of the transmission coefficient described in Section 4.2.1.

4.3 Results and Discussion

4.3.1 Waves

A minimal impact on the surface waves was expected due to the small ratio between the monopile diameter (7 m) and the wavelength (41.2 m to 87.5 m) in the Kingston Basin during the storm event. Typically, diffraction and reflection are significant processes when $D/L > 0.2$ (Isaacson, 1979), where D is the diameter of the structure and L is the wavelength. The wave conditions in this case correspond to $0.08 \leq D/L \leq 0.17$, indicating that reflection and diffraction are negligible processes. Scattering of wave energy and pile group effects are estimated to be small as a result of the large spacing (1 km) between piles (Alari and Raudsepp, 2012).

The offshore wind farm's impact on waves was assessed statistically and by comparing the percent change in significant wave height between the validated model without the farm and the model with the wind farm. Statistical representations of wave impacts are provided in Table 4.1 with comparison locations identified in Figure 4.4. Significant wave height (H_s) and peak wave period (T_p) before and after implementation of the wind farm are compared in Table 4.1. The average of these values from each location was taken where RMSE is the root-mean-squared error and R is the correlation coefficient. Table 4.1 vales indicate small changes occurring to waves in the near-field. The percent change ΔH_s was determined as follows:

$$\Delta H_s = \left(\frac{H_{s\_f} - H_{s\_n}}{H_{s\_n}}\right) \times 100\% \quad (4.4)$$

where H_{s_n} is the significant wave height of the model of the Kingston Basin in its present, natural state (m) and H_{s_f} is the significant wave height of the model with the added wind farm (m). Contour lines that indicate the percent change between Main Duck Island and Wolfe Island are shown in Figure 4.5. The largest changes in H_s are increases of < 0.15 m and are seen within the wind farm area and at the shallow headlands of Big Sandy Bay at the peak of the storm event,

where southwesterly winds are over 18 m s^{-1}. The increases and decreases in H_s vary based on the complex bathymetry of the basin, which focuses the refracted energy of waves due to the obstacles, to the shallower regions including shoals. Slight far-field changes in significant wave height of < 2% and near-field changes of < 3% are produced by the model. The largest far-field impacts occur during the southwesterly winds (Figure 4.5), as waves are influenced by the entire length of the wind farm.

Table 4.1: Average Wave Statistics over the farm from Jan 16-18, 2012

RMSE H_s (m)	0.02
RMSE T_P (s)	0.04
R H_s	0.99
R T_P	1.00

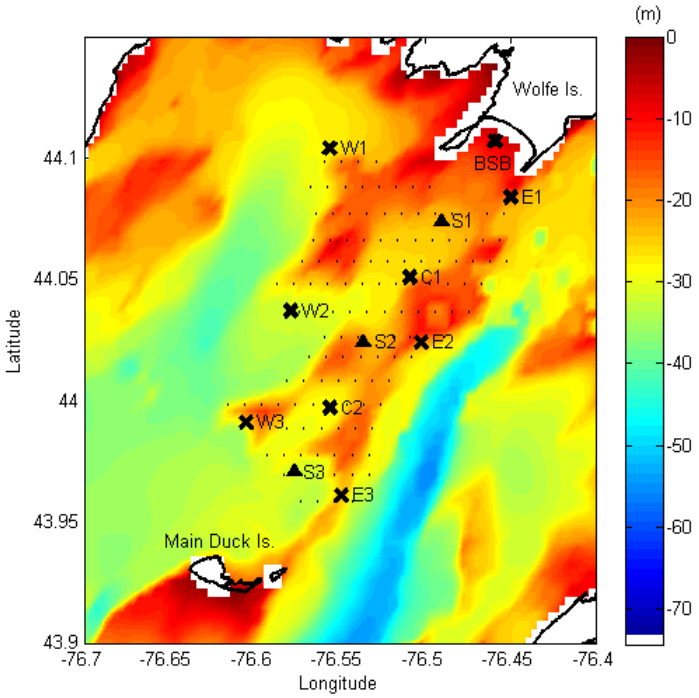

Figure 4.4: Bathymetry of the proposed wind farm area. Wind turbine locations are indicated by the small dots and wave and current comparison locations are marked with an x (W1-3, C1-2, E1-3 and BSB). The spectral comparisons were made at the locations marked with triangles (BSB and S1-3).

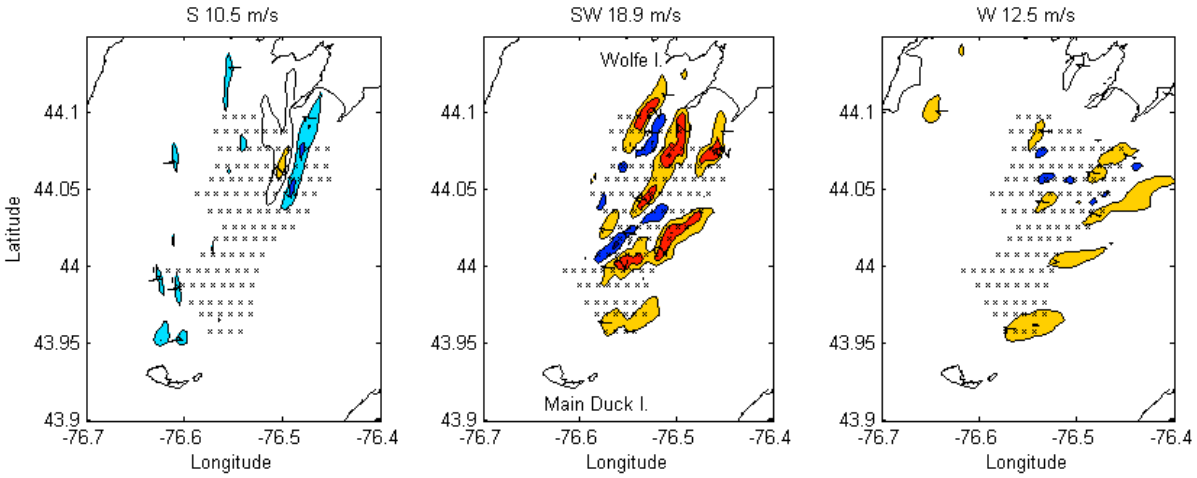

Figure 4.5: Percent reduction of significant wave height in Kingston Basin due to implementation of a wind farm, for three different storm conditions. Each contour line unit is in % and a positive value (warm colours) represents an increase in significant wave height and a negative value (cold colours) represents a decrease. Wind direction and speed for each plot is indicated.

In the Baltic Sea, Alari and Raudsepp (2012) found that significant wave heights were reduced marginally, 1% below 10 m isobaths within a 55 turbine farm with 5 m diameter and a spacing of 1 km. In the UK, on the north coast of Cornwall, Millar et al. (2007) found a probable reduction in significant wave height near the coast of less than 2 cm while studying various transmission coefficients and various wave parameters. Other studies have found larger impacts on significant wave heights (up to 50 cm at 20 m behind a 7 m monopile; Ponce de Léon et al., 2011), although these results were attained in the wake of the turbine and lost significance after the first 20 m. Decreases in significant wave height due to wind farm construction found in this chapter are therefore as expected.

The loss of wave spectral energy due to the turbines is shown in Figure 4.6 at four locations identified in Figure 4.4 (BSB and S1-3), during the three wind conditions identified in Figure 4.3. The energy due to the swell from the main basin of the lake (< 0.2 Hz) increases by up

to 5% through the middle of the wind farm while higher frequency, wind-sea energy (> 0.2 Hz) from waves generated inside the Kingston Basin diminish in some locations. This exchange in energy can be attributed to the refraction of larger waves into the wind farm as a result of the turbine piles. The higher frequency energy is reduced by up to 3% in some locations as a result of the reduced effective fetch for waves generated inside the basin and increased whitecapping dissipation. Outside the wind farm, on the downwind side, Big Sandy Bay (BSB) and other coastal areas have the smallest changes in wave energy and the impact of the wind farm on waves is mostly within the farm area.

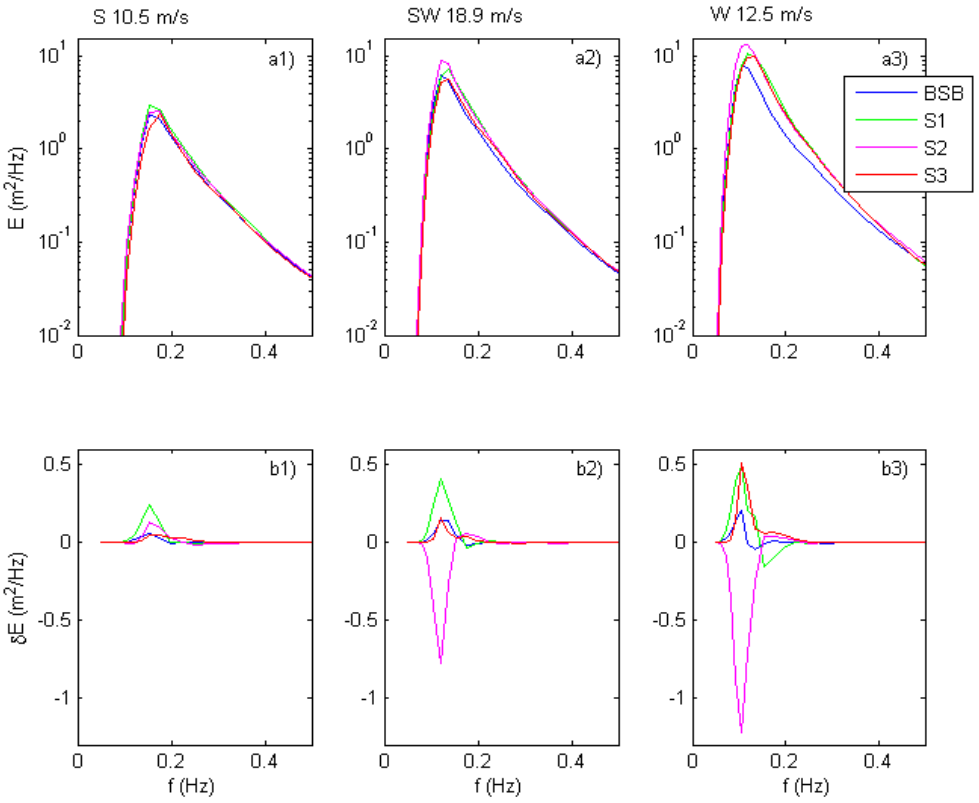

Figure 4.6: Simulated wave spectra at various locations during three different wind conditions (indicated) through the proposed center of the wind farm for three different storm conditions (a1-a3) and difference in wave spectral energy between the wind farm model and the model without a wind farm. A positive spectrum indicates an increase in spectral energy, while a negative spectrum indicates a decrease.

For comparison, Ponce de Léon et al. (2011) found that wave energy due to a wind farm of 90 turbines at 540 m spacing, with wave periods of 15 s, decreased by 16% in the near-field and by 5% in the far-field. In this chapter, with a greater pile spacing of 1 km and lower wave periods of 6-7 s, we find small changes in wave energy of < 5 % in the near-field and negligible changes in the far-field.

4.3.2 Circulation

The impact of a wind farm on the circulation through the Kingston Basin is greater than expected due to its complex bathymetry. Statistics, including RMSE and R, were computed and are shown in Table 4.2 in order to compare the circulation before and after wind farm implementation to the model. The locations, of which these statistics were predicted, are the same as those used to compare waves (see Figure 4.4). The residuals between depth averaged current magnitude and direction (see Figure 4.7) suggest that an offshore wind farm would bring slight changes to the currents, although the circulation patterns would remain unchanged. The majority of impacts to circulation occur in the near-field, with changes in current magnitude of up to +0.08 m s^{-1} and -0.05 m s^{-1} across the farm, and a RMSE of direction change of 19° at the northern end of the wind farm. Some areas in the far-field show changes of up to +0.05 m s^{-1}, during the westerly wind condition (Figure 4.7, c3) in shallow areas (< 10 m near the headlands surrounding Big Sandy Bay). The northernmost end of the wind farm (Figure 4.8) has the largest changes to current velocity during southern wind conditions. The wind farm has the highest percentage changes during strong winds, since the circulation in Kingston Basin becomes strongest and most well defined during storm conditions (Chapter 3).

Table 4.2: Average Flow Statistics over the farm from Jan 16-18, 2012

RMSE $\|u\|$ (m s^{-1})	0.01
RMSE θ_u (°)	19
R $\|u\|$	0.91
R θ_u	0.93

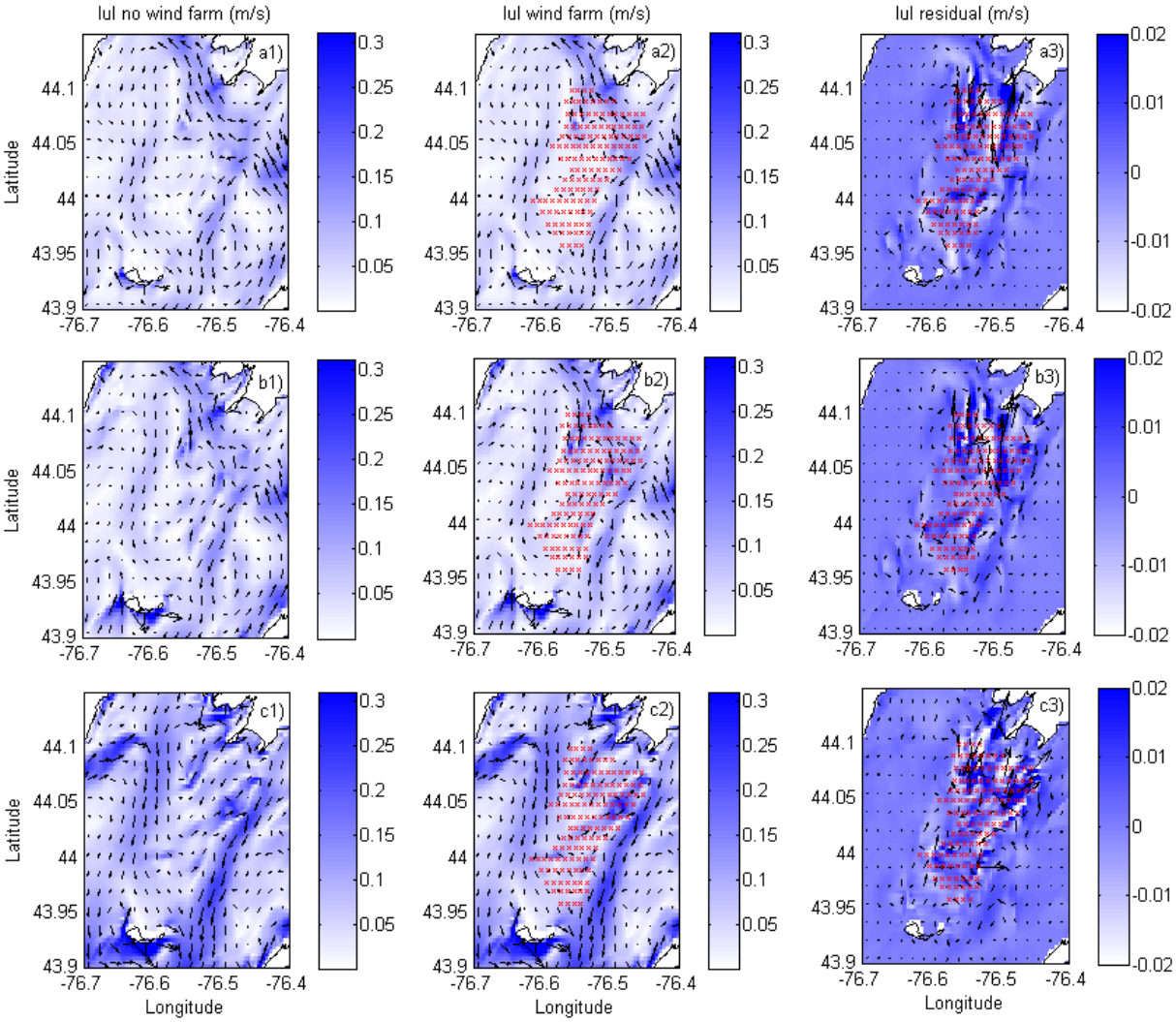

Figure 4.7: Depth averaged current magnitude ($|u|$) and direction (vectors) in the study area: (1) without a wind farm, (2) with wind farm, and (3) the residual difference for three different storm conditions (a-c) corresponding to the times indicated in Figure 4.3. Turbines are indicated by the red dots. Note the change in color scale in a3-c3.

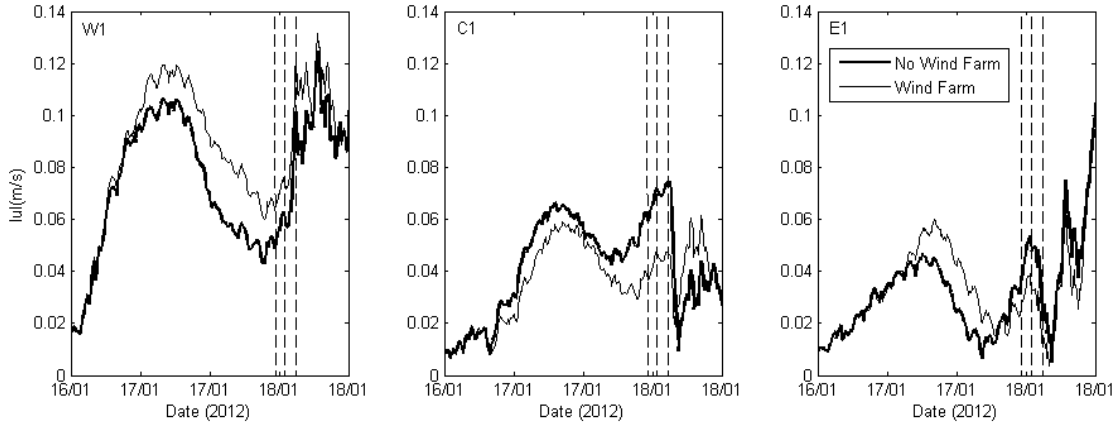

Figure 4.8: Depth averaged current magnitude (|*u*|) at three locations indicated in the top left corner (see Figure 4.4). Vertical lines indicate the times shown in Figures 4.5 and 4.6. The thick line represents simulated results without the implementation of a wind farm and the thin line represents the results with a potential wind farm implemented.

ETSU (2002) found that detectable changes within a wind farm on the UK coast consisting of 30 piles with a foundation diameter of 5 m and a spacing of 400 m, dissipated 400 m downstream of the structures with the largest reduction in flow of 0.05 m s^{-1} and largest increase of 0.02 m s^{-1}. Changes in flow directions were small, less than 1.5°. Baird (2011) suggested changes in circulation can be expected in the Great Lakes ranging from 2-4% in the near-field and < 1% in the far-field based on available sources (e.g. Cooper and Beiboer, 2002; CEFAS, 2006). The changes that have been predicted in this chapter are higher (in some locations up to 50%) due to slight changes to the complex circulation patterns (e.g. gyres) within the wind farm area, which are driven by wind and topography (Chapter 3). The circulation in the near-field balances the reductions at some locations with increases in flow at others, allowing the overall circulation of the Kingston Basin to remain relatively unchanged.

4.4 Conclusions

The effects of an offshore wind farm on waves and circulation in the Kingston Basin of eastern Lake Ontario has been numerically modelled as a contribution toward understanding wind farm impacts in the Great Lakes. Far-field changes (1 km or more outside the farm area) in significant wave height of < 2% can be expected in coastal areas including the shores of Wolfe Island and changes of < 3% can be expected in the near-field (less than 1km from the farm and inside the farm area). The majority of impacts to circulation in the Kingston Basin can be expected to occur in the near-field, with small changes in current velocity of < 0.08 m s^{-1} and the RMSE of direction change to be approximately 19°. Some areas in the far-field near Wolfe Island exhibit changes of ~ 0.05 m s^{-1}, although basin-scale circulation patterns are minimally affected. The majority of changes to surface waves and wind-driven currents are due to wind farm position with respect to wind direction and the re-direction of flows and waves through the wind farm.

Future research should extend the present study to modelling the impact of the changes to waves and currents on sediment transport processes (e.g. scour or deposition at the base of monopiles). Sediment processes could be disturbed by wind farms (e.g. Nielsen and Hansen, 2007) and should be evaluated for Lake Ontario in future studies. An important process to consider in mid-to high latitude lakes is floating freshwater ice. Ice modelling has been studied in detail for the Great Lakes (Oveisy et al., 2013; Wang et al., 2010) and applying numerical models to offshore wind applications would provide insight to their impacts on ice processes (e.g. ice circulation and ice forces). Wake effects due to offshore wind turbines have been studied using satellite radar (e.g. Christiansen and Hasager, 2005; Barthelmie et al., 2003) and should be considered in future modelling studies. Reductions in surface wind speed over wind farms are typically < 10% (Christiansen and Hasager, 2005) with some recovery beyond the farm, therefore

further influencing wave generation and dissipation downwind of each turbine monopile. The number of turbines, turbine spacing and shape of the wind farm are therefore likely to be very important decisions that influence the surface waves and circulation inside the farm and surrounding coastal region.

Chapter 5

Conclusions

Five storm events were simulated using two model domains covering Lake Ontario and the Kingston Basin. The models were validated using measurements during winter storm events, and the results were used to further understand the surface wave and flow fields through the Kingston Basin. The validated lake-wide model was then used to assess the impacts of a potential offshore wind farm. The following findings were established:

- Overall, the open boundary driven model provided a slightly better representation of the waves (average correlation coefficient of 0.90 for boundary driven compared to 0.83 for the lake-wide model), due to local winds and wave boundary conditions. A lake-wide model, however, resulted in a much more accurate representation of the magnitude and direction of currents (by up to 44%). The complexity of the circulation at the boundary in the KBM was not captured, since it was forced with a spatially uniform boundary condition. The lake-wide domain allowed for the full circulation pattern of the lake to develop and provide a better input to the sub-domain.

- Waves propagating from the main basin into the Kingston Basin lose approximately 17-19% of their energy density due to breaking and refraction over Duck-Galloo Ridge. Within the basin, waves are composed of both swell and wind-sea spectral components. During the largest storms identified, wave directions were near-perpendicular to the

Ridge, causing swell to refract and enter the basin through the Simcoe Island and St. Lawrence Channels surrounding Main Duck Island.

- The depth averaged current speed in the Simcoe Island Channel (41.2 m deep) during peak storm conditions were low (0.02-0.04 m s^{-1}) and directed into the basin, while speeds in the St. Lawrence Channel (56.2 m deep) were much stronger and up to 0.2 m s^{-1} from the Kingston Basin.

- The impacts of waves on the circulation patterns at the basin scale are negligible, since shoals are typically too deep (e.g. 20m) relative to the wavelength and period (e.g. 7-10 s) and breaking does not occur, which would generate large-scale wave-driven flows.

- A method for assessing the effects of an offshore wind farm on waves and circulation in the Kingston Basin of eastern Lake Ontario was applied. Far-field changes in significant wave height of < 2% can be expected in coastal areas, including the headlands of Big Sandy Bay, Wolfe Island, and changes of < 3% can be expected in the near-field. The majority of impacts to circulation in the Kingston Basin occur in the near-field, with small changes in current velocity of < 0.08 m s^{-1} (up to 50%) and the RMSE of direction (19°). Some areas in the far-field near Wolfe Island exhibit changes of ~ 0.05 m s^{-1} (approximately 30%), although overall circulation patterns are not affected. The majority of changes to surface waves and wind-driven currents are due to wind farm position with respect to wind direction and the re-direction of flows and waves throughout the wind farm.

Future research should extend the present research to modelling sediment transport and coupling between surface dynamics and temperature stratification. Modelling the impact of offshore wind farms on sediment transport processes would then be possible. Sediment processes could be disturbed by wind farms and should be evaluated for Lake Ontario in future studies, especially since the ADCP backscatter observations show sediment resuspension may occur during large storm events (Appendix A, Figure A.1). Based on the predicted changes in waves and current speed and direction, sediment dynamics may be affected by an offshore wind farm. Ice modelling has been studied in detail for the Great Lakes and applying numerical models to offshore wind applications would provide insight to their impacts on ice processes (e.g. ice circulation and ice forces). Wake effects due to offshore wind turbines have been studied using satellite radar and should be considered in future modelling studies. There are also other techniques for represent wind farms in wave and hydrodynamic models. The adequacy of each of these techniques for freshwater wind farm applications should be assessed for future consideration. The simulation of longer time periods (over the course of several months) might help shed more light on wind farm impacts, especially when considering sediment transport and during non-storm periods.

References

Alari, V., Raudsepp, U. (2012). Simulation of Wave Damping Near Coast due to Offshore Wind Farms. *J. Coast. Res.* 28(1), 143-148.

Baird. (2011). *Offshore Wind Power Coastal Engineering Report*. Prepared for the Ontario Ministry of Natural Resources May, 2011.

Barthelmie, R.J., Folkerts, L., Ormel, F.T., Sanderhoff, P., Eecen, P.J., Stobbe, O., Nielsen, N.M. (2003). Offshore Wind Turbine Wakes Measured by Sodar. *J. Atm. and Oceanic Tech.* 20, 466-477.

Bedford, K.W., Schwab, D.J. (1991). Wind-Induced Hypolimnion Exchange in Lake Ontario's Kingston Basin: Potential Effects on Oxygen. *J. Great Lakes Res.* 24 (1), 145-151.

Beletsky, D., Saylor, J.H., Schwab, D.J. (1999). Mean Circulation in the Great Lakes. *J. Great Lakes Res.* 25(1), 78-93.

Bennet, J.R. (1974). On the Dynamics of Wind-Driven Lake Currents. *J. Phys. Ocean.* 4, 400-414.

Booij, N., Ris, R.C., Holthuijsen, L.H. (1999). A Third-Generation Wave Model for Coastal Regions 1.Model Description and Validation. *J. of Geophys. Res.*, Vol. 104, 7649-7666.

Boyce, F.M., Donelan, M.A., Hamblin, P.F., Murthy, C.R., Simons, T.J. (1989). Thermal Structure and Circulation in the Great Lakes, *Atmosphere-Ocean.* 27 (4), 607-642.

Breton, S., Moe, G. (2008) Status, Plans and Technologies for Offshore Wind Turbines in Europe and North America. *Renewable Energy*. 34 (2009) pp.646-654.

CBC News (2011) *Ont. Declares Moratorium on Off-Shore Wind Farms*. Available at: <http://www.cbc.ca/news/canada/toronto/story/2011/02/11/ont-wind-farms.html>.[February 11, 2011].

CEFAS. (2006). *Scroby Sands Offshore Wind Farm Coastal Processes Monitoring. Final Report.* Report prepared for the Department of Trade and Industry, UK. Contract Ref. No. AE0262.

Christiansen, M.B., Hasager, C.B. (2005). Wake Effects of Large Offshore Wind Farms Identified from Satellite SAR. *Remote Sensing of Env.* 98(2005), 251-268.

Cooper, B., Beiboer, F. (2002). *Potential Effects of Offshore Wind Developments on Coastal Processes.* Report Submitted to Department of Trade and Industry, UK. Report No. ETSU W/35/00596/00/REP.

Danish Energy Agency (DEA). (2006). *Offshore Wind Farms and the Environment - Danish Experience from Horns Rev and Nysted*. Published by the Danish Energy Authority November, 2006.

Delft-3D User Manual. (2011). *Delft3D-FLOW Simulation of multi-dimensional hydrodynamic flows and transport phenomena, including sediments, User Manual.Deltares*: The Netherlands.

Dingemans, M.W., Radder, A.C., de Vriend, H.J. (1987). Computation of the Driving Forces of Wave-Induced Currents. *Coast. Eng.* 11, 539-563.

Elias, E.P.L., Gelfenbaum, G., Van der Westhuysen, A.J. (2012). Validation of a Coupled Wave-Flow Model in a High-Energy Setting: The Mouth of the Columbia River. *J. of Geophys. Res.* 117, C09011, doi:10.1029/2012JC008105.

Elias, E.P.L., Walstra, D.J.R., Roelvink, J.A., Stive, M.J.F., Klein, M.D. (2000). Hydrodynamic validation of Delft3D with field measurements at Egmond.Coastal Engineering.

ETSU. (2002). *Potential Effects of Offshore Wind Developments on Coastal Processes.* ETSU W/35/00596/00/REP. Prepared by ABPmer and METOC.

Gilbert, R., Hartling, J.W. (1999). Spacial Distribution of Surficial Sediments in Part of the Kingston Basin of Northeastern Lake Ontario, Canada.NRC: Canada.

Gorrell, L., Raubenheimer, B., Elgar, S., Guza, R.T. (2010). SWAN Predictions of Waves Observed in Shallow Water Onshore of Complex Bathymetry. *Elsevier B.V.*: USA.

Hamblin, P.F. (1982). On the Free Surface Oscillations of Lake Ontario. *Limnology Ocean.* 27, 1039-1049.

Hayashi, T., Hattori, M., Kano, T., Shirai, M. (1966). Hydraulic Research on the Closely Spaced Pile Breakwater. *Coastal Eng.* 50, 873-884.

Huang, A., Rao, Y.R., Lu, Y., and Zhao, J. (2010). Hydrodynamic Modeling of Lake Ontario: An Intercomparison of Three Models, *J. Geophys. Res., 115*, C12076, doi:10.1029/2010JC006269.

Isaacson, M. (1979). *Waves Forces on Compound Cylinders*. Proc, Civil Engineering in the Oceans IV, ASCE, San Francisco, Vol. I.

Kamphuis, J.W. (2010). *Introduction to Coastal Engineering and Management.* Advanced Series on Ocean Engineering, Vol. 30.

Lesser, G.R., Roelvink, J.A., van Kester, J.A.T.M., Stelling, G.S. (2004). Development and Validation of a Three-Dimensional Morphological Model. *Coastal Eng.*: The Netherlands.

Manwell, J.F., Elkinton, C.N., Rogers, A.L., McGowan, J.G. (2007). Review of Design Conditions Applicable to Offshore Wind Energy Systems in the United States. *Reviews*. 11(2), 210-234.

McCombs, M.P., Mulligan, R.P., Boegman, L., Rao, Y.R. (2013). Modelling Winter Storm Surface Waves and Wind-Driven Circulation in Eastern Lake Ontario. *J. Great Lakes Res.*, submitted.

McCombs, M.P., Mulligan, R.P., Boegman, L., Rao, Y.R. (2013). Wave Propagation and Growth in the Kingston Basin of Eastern Lake Ontario. *CSCE 4th Special Conference on Coastal, Estuary and Offshore Engineering.* COS-009.

Millar, D.L., Smith, H.C.M., Reeve, D.E. (2007). Modelling Analysis of the Sensitivity of Shoreline Change to a Wave Farm. *Ocean Eng.* 34, 884-901.

Mulligan, R.P., Hay, A.E., Bowen, A.J. (2010).A Wave-Driven Jet Over a Rocky Shoal. *J. of Geophys. Res.*, 115, C10038.

National Geophysical Data Center. (2011). *Marine Geology & Geophysics Shoreline / Coastline Data*. http://www.ngdc.noaa.gov/mgg/shorelines/shorelines.html

Nielsen, A.W., Hansen, E.A. (2007). Time-Varying Wave and Current-Induced Scour Around Offshore Wind Turbines. *Proc. 26th Int. Conf. on Offshore Mechanics and Artic Eng.* ASME, 10-15 June, 2007, San Diego, California, USA, 10pp.

NOAA Great Lakes Environmental Research Laboratory. (2013). *Great Lakes Coastal Forecasting System, GLCFS*. http://www.glerl.noaa.gov/res/glcfs/

NOAA National Geophysical Data Center. (2013). *GEODAS Grid Translator.* http://www.ngdc.noaa.gov/mgg/gdas/gd_designagrid.html

ORTECH Environmental. (2010). Request for Proposal: Wolfe Island Shoals Offshore Windfarm Permitting and Field Investigation Services.

Oveisy, A., Boegman, L., Imberger, J. (2012). Three-Dimensional Simulation of Lake and Ice Dynamics During Winter. *Limnol. Oceanogr.* 57(1), 2012, 43-57.

Paturi, S., Boegman, L., Rao, Y.R. (2012). Hydrodynamics of Eastern Lake Ontario and upper St. Lawrence River. *J. Great Lakes Res.* 38, 194-204.

Pickett, R.L. (1980). Observed and Predicted Great Lakes Winter Circulations. *J. of Phys. Ocean*. 10, 1140-1146.

Ponce de Leon, S., Bettencourt, J.H., Kjerstad, N. (2011). Simulation of Irregular Waves in an Offshore Wind Farm with a Spectral Wave Model. *Continental Shelf Res.* 31(2011), 1541-1557.

Prakash, S., Atkinson, J.F., Green, M.L. (2007). A Semi-Lagragian Study of Circulation and Transport in Lake Ontario. *J. of Great Lakes Res.* 33(4): 774-790.

Rao, D.B., Murty, T.S. (1970). Calculation of the Steady-State Wind Driven Circulation in Lake Ontario. *Arch. Meteorol. Geophys. Bioklimatol.* Ser. A19: 195-210.

Rueda, F.J., Vidal, J. (2009). Currents in the Upper Mixed Layer and in Unstratified Water Bodies, in Editor-in-Chief: Gene E. Likens (Ed.), *Encyclopedia of Inland Waters*. pp. 568-582.

Schwab, D.J., Bedford, K.W. (1994). Initial Implementation of the Great Lakes Forecasting System: A Real-Time System for Predicting Lake Circulation and Thermal Structure. *Water Pollution Res. J. of Canada* 29(2/3):203-220.

Schwab, D.J., Bennett, J.R., Liu, P.C., Donelan, M.A. (1984). Application of a Simple Numerical Wave Prediction Model to Lake Erie. *J. Geophys. Res.* 89, 3586-3592.

Shore, J.A. (2009).Modelling the Circulation and Exchange of Kingston Basin and Lake Ontario with FVCOM. *Elsevier: Canada*.

Simons, T.J. (1974). Verification of Numerical Models of Lake Ontario I. Circulation in Spring and Early Summer. *J. Phys. Ocean.* 4:507-523.

Simons, T.J., Murthy, C.R., Campbell, J.E. (1985). Winter Circulation in Lake Ontario. *J. Great Lakes Res.* 11:423-433.

Sly, P.G., Prior, J.W. (1984). Late glacial and postglacial geology in the Lake Ontario basin. Can. J. Earth Sci. 21. 802-821 (1984).

Soulsby, R.L., Hamm, L., Klopman, G., Myrhaug, D., Simons, R.R., Thomas, G.P. (1993). Wave-Current Interaction Within and Outside the Bottom Boundary Layer. *Coast. Eng.* 21: 41-69.

Stive, M.J.F., Wind, H.G. (1986). Cross-Shore Mean Flow in the Surf Zone. *Coast. Eng.* 10, 325-340.

Sumer, B.M., Fredsoe, J. (1997). *Hydrodynamics Around Cylindrical Structures*. World Scientific Publishing Co. Pte. Ltd., Singapore.

Sumer, B.M., Fredsoe, J. (2002). *The Mechanics of Scour in the Marine Environment.* World Scientific Publishing Co. Pte. Ltd., Singapore.

Svendsen, I.A. (1985). Mass Flux and Undertow in a Surf Zone, *Coast. Eng.* 10 (3), 299-307.

Tsanis, I.K., Masse, A., Murthy, C.R., Miners, K. (1991). Summer Circulation in the Kingston Basin, Lake Ontario. *J. of Great Lakes Res.* 17(1), 57-73.

Tsanis, I.K., Murthy, C.R. (1990). Flow Distribution in the St. Lawrence River System at Wolfe Island, Kingston Basin, Lake Ontario. *J. of Great Lakes Res.* 16(3), 352-365.

Wang, J., Hu, H., Schwab, D., Beletsky, D., Clites, A., Leshkevich, G. (2010). Development of the Great Lakes Ice-Circulation Model (GLIM): Application to Lake Erie in 2003-2004. *J. Great Lakes Res.* 36: 425-436, doi:10.1016/j.jglr.2010.04.002.

Appendix A

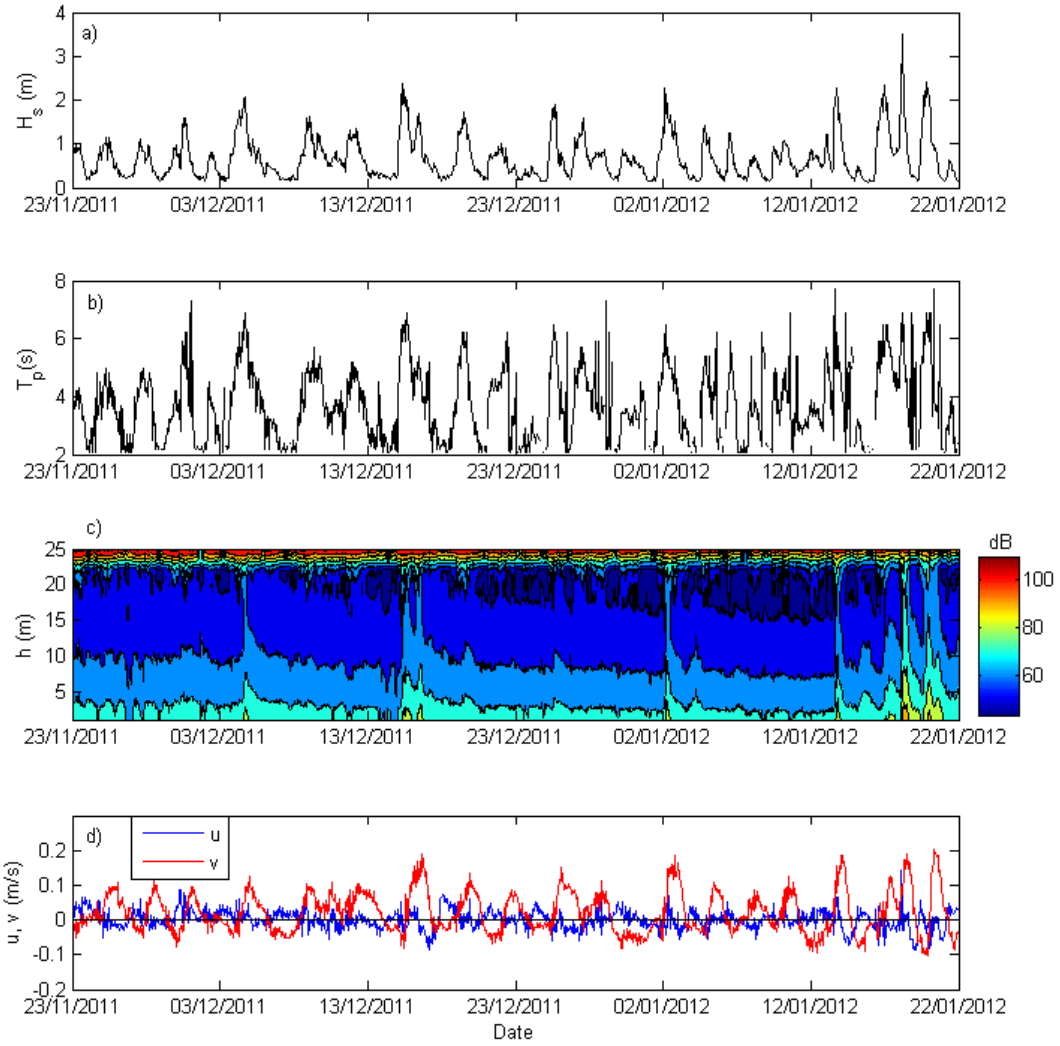

Figure A.1: a) Significant wave height (H_s) observed at site A (Chapter 3). b) Peak wave period (T_p) observed at site A (Chapter 3). c) Acoustic backscatter measured at site A (Chapter 3) where *h* is the height from the bottom. d) Depth averaged current velocity in the *u* and *v* directions. Increases in the acoustic backscatter likely represent sediment resuspension into the water column as they are well correlated with increases in significant wave height and current velocity. OBS (Optical Backscatter Sensor) observations were also collected during the 2011-12 winter period by Environment Canada (not shown).

Appendix B

Table B.1: Table of Parameter Values Used in Numerical Models

Symbol	Description	Value Used	Units
Delft3D – FLOW Module			
Δt	Time Step	1	min
C_d	Wind Drag Coefficient (First Breakpoint)	0.00063 (at 0 m/s)	
C_d	Wind Drag Coefficient (Second Breakpoint)	0.00723 (at 100 m/s)	
C	Chezy Roughness	65	$m^{1/2}\ s^{-1}$
ν_H	Horizontal Eddy Viscosity	1	$m^2\ s^{-1}$
	Threshold Depth	0.5	m
ρ	Water Density	1000	$kg\ m^3$
SWAN			
f	Frequency Space	0.05 - 1	Hz
M_f	Number of Frequency Bins	24	
ρ	Water Density	1000	$kg\ m^3$
	Minimum Depth	0.5	m
α_b	Depth-Induced Breaking (B&J Model) Alpha	1	
γ_b	Depth-Induced Breaking (B&J Model) Gamma	0.73	
	Bottom Friction (Jonswap)	0.067	$m^2\ s^{-3}$
	Coupling Interval	60	min

Appendix C

Table C.1: Table of Parameters Used for Sensitivity Analysis of the KBM

Symbol	Description	Range	Units
v_H	Horizontal Eddy Viscosity	0.1 - 10	$m^2\ s^{-1}$
C	Chézy Roughness	46 - 92	$m^{1/2}\ s^{-1}$
Dy x Dx	Grid Resolution	380x270 and 130x90	m

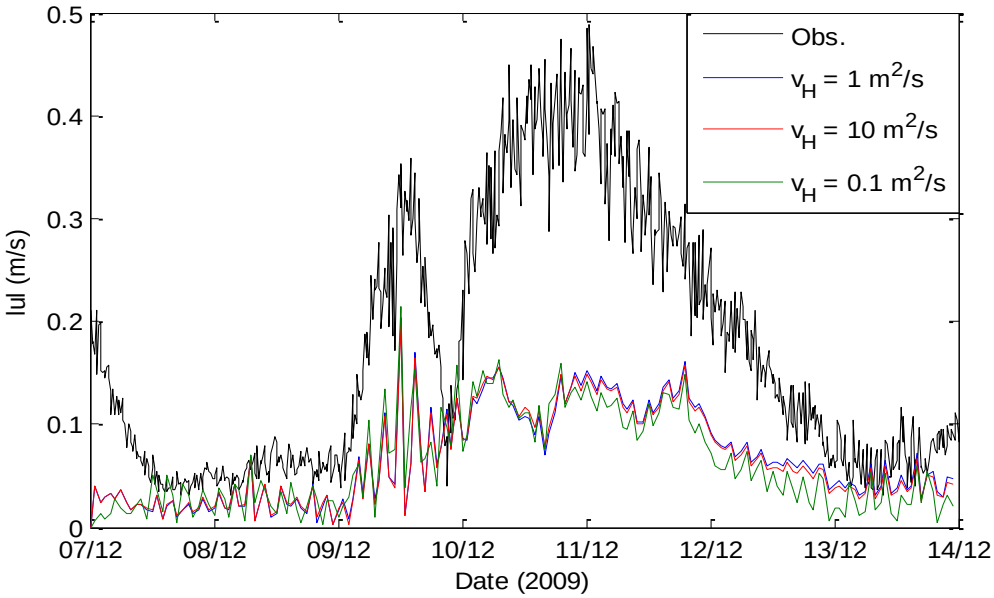

Figure C.1: Sensitivity analysis of horizontal eddy viscosity in an attempt to better represent current velocity magnitude using the KBM in Chapter 3.

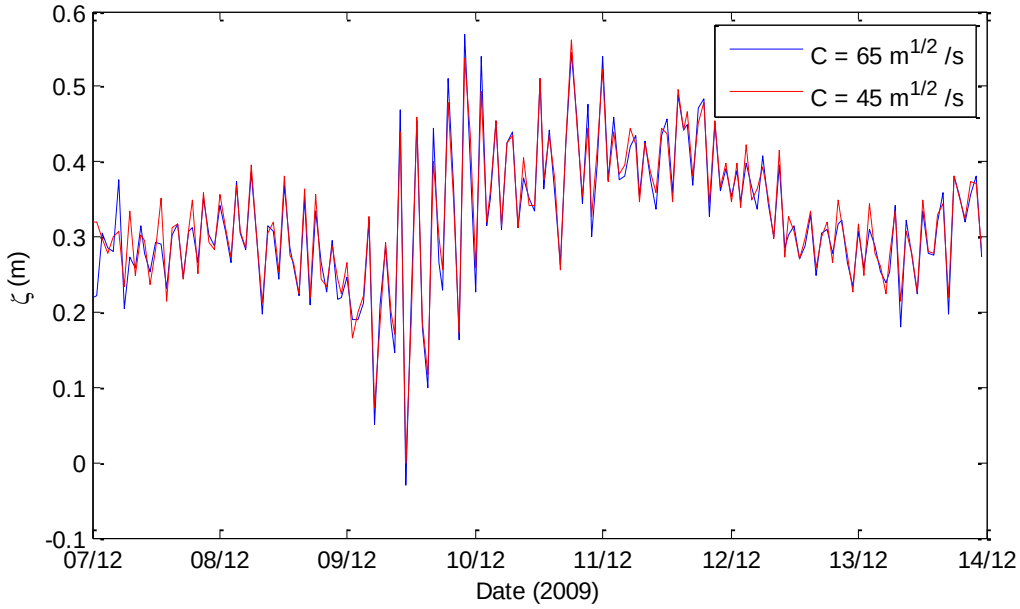

Figure C.2: Sensitivity analysis of the Chézy Roughness coefficient in an attempt to better represent seiching (reduce water level oscillations). A Chézy value of 92 (not shown) increased water level oscillations, increasing the error between simulated and observed water levels.

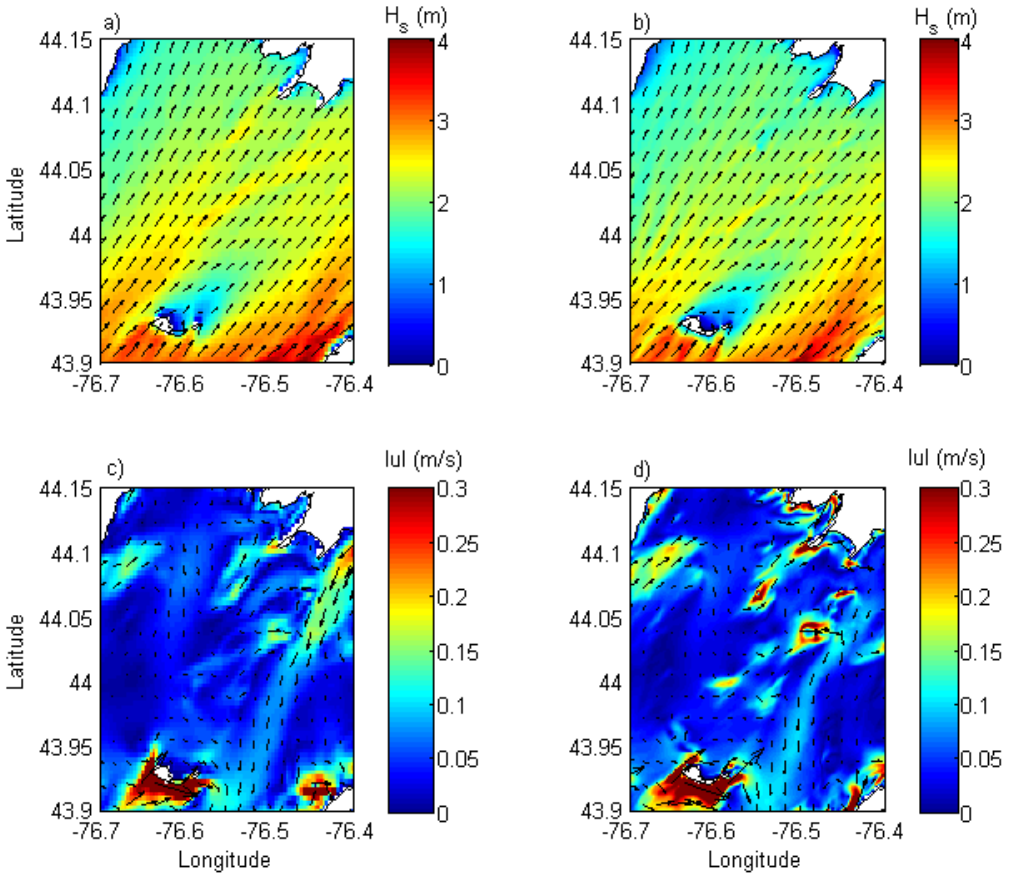

Figure C.3: Grid sensitivity analysis of significant wave height (H_s) and depth-averaged current velocity magnitude ($|u|$). Subplots a and c represent the model resolution of 380 m x 270 m, and subplots b and d represent model resolution of 130 m x 90 m.